Uncertainty in damage assessment and remaining life prediction of engineering materials used in petrochemical industry

Ashok Kumar Ray
Materials Science and Technology Division
CSIR-National Metallurgical Laboratory
Jamshedpur-831007, India
Email: asokroy@nmlindia.org

Petrochemistry 2014: 27-29 October, Las Vegas, USA

Team members

A. K. Ray , N. Roy, A. Raj[1], M. Matwa[2], A. Davuluri[2], A. Kumari[3], P.K. Sharma[4], D. Mundhada[5], B.N. Roy[6]

Materials Science and Technology Division

CSIR-National Metallurgical Laboratory

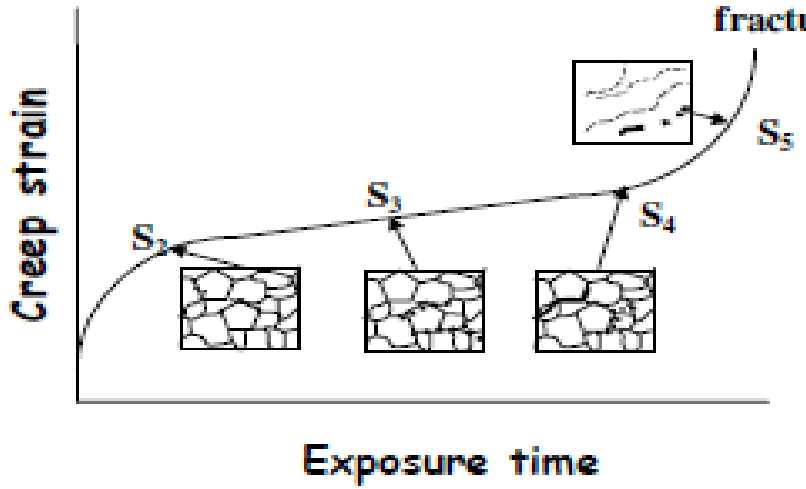
Jamshedpur-831007, India

- 1.R.V.S. College of Engineering and Technology, Jamshedpur-831012, India
- 2.Indian Institute of Technology, Kharagpur-721302, India
- 3.Indian Institute of Technology, (BHU) Varanasi-221005, India
- 4.National Institute of Technology, Rourkela-769008, India
- 5.National Institute of Technology, Warangal-506004, India
- 6.Bihar Institute of Technology, Sindri-828123, India

Petrochemistry 2014: 27-29 October 2014, Las Vegas, USA

Part I : Structural integrity and uncertainty in creep damage assessment of service exposed reformer tubes

Material	**:Primary reformer tube of grade HP40 (25 Cr-35Ni-Nb with 0.4% C)**
Number of years of service exposure	**:11 years**
Operating hoop stress	**:13.46 Mpa**



Damage State	Description
S_1	Virgin
S_2	Isolated cavities
S_3	Aligned cavities
S_4	Linked cavities
S_5	Macro crack
S_6	Fracture

Fig.1 A schematic representation of the nature of **damage evolution in material subjected to creep loading and the phases** used to represent the same.

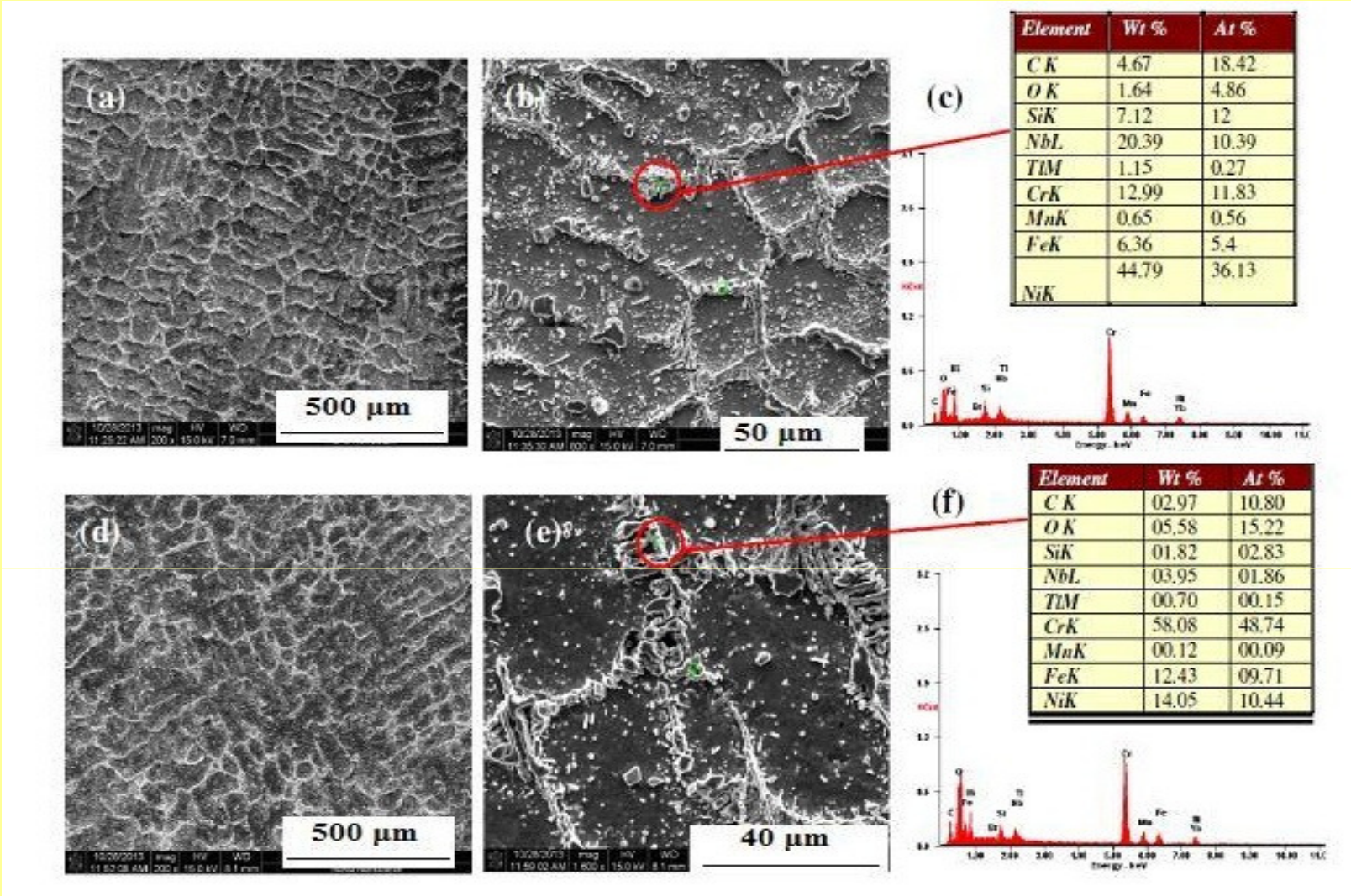
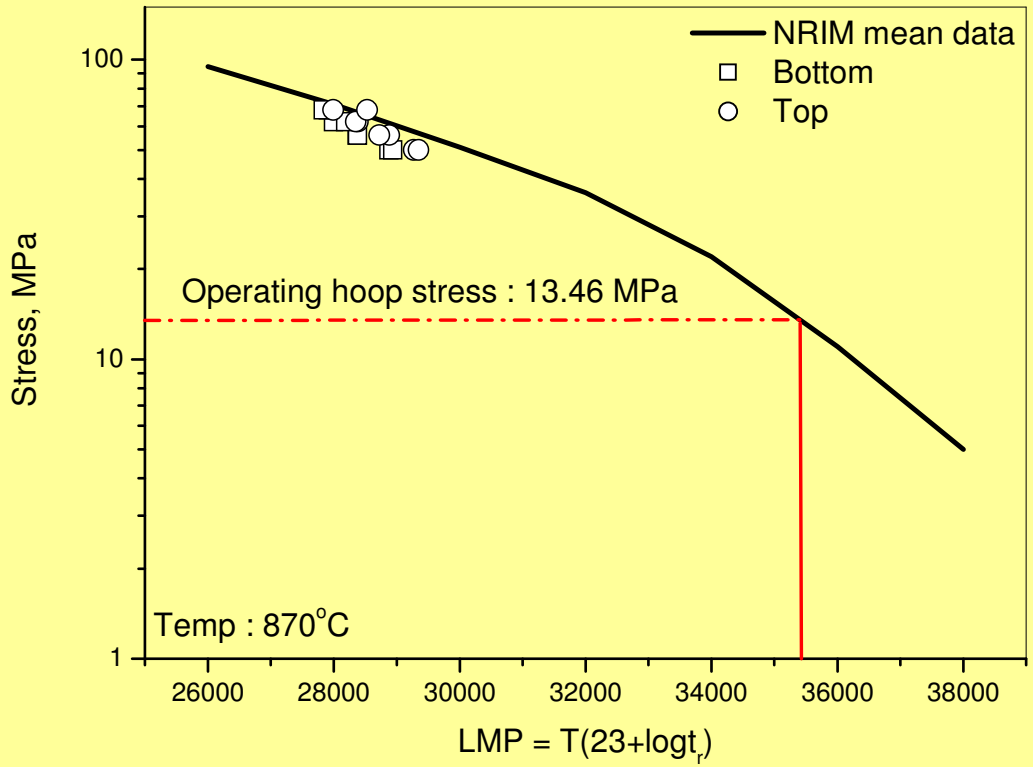


Fig.2 SEM micrograph revealing microstructure of as received **top and bottom portions of the reformer tube** with EDAX analysis of **Cr and Nb rich precipitates**


NRIM mean data
Bottom
Top
Operating hoop stress : 13.46 MPa
Temp : 870°C
Stress, MPa
100
10
1
26000
28000
30000
32000
34000
36000
38000
LMP = T(23+logt_r)

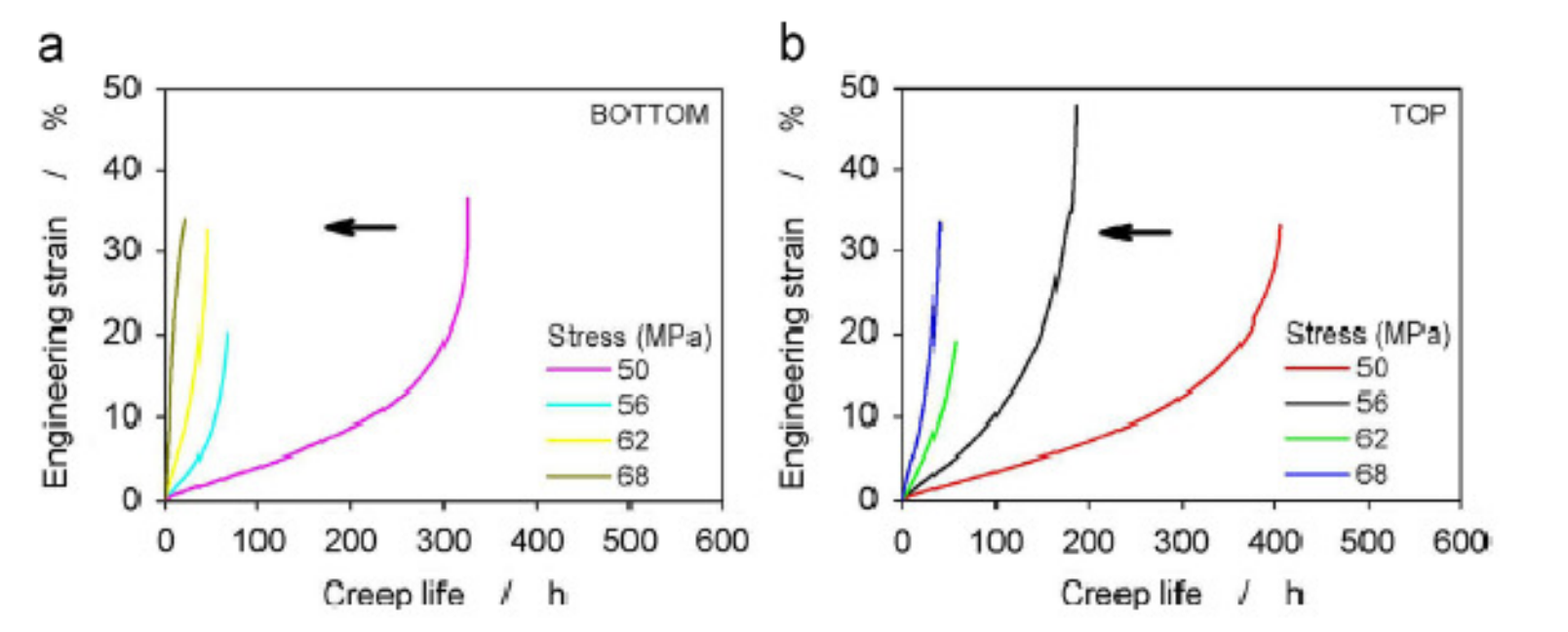


Fig.3a Experimental creep curves at **four different stress** levels for the (a) **bottom** and (b) **top** portion of tubes.

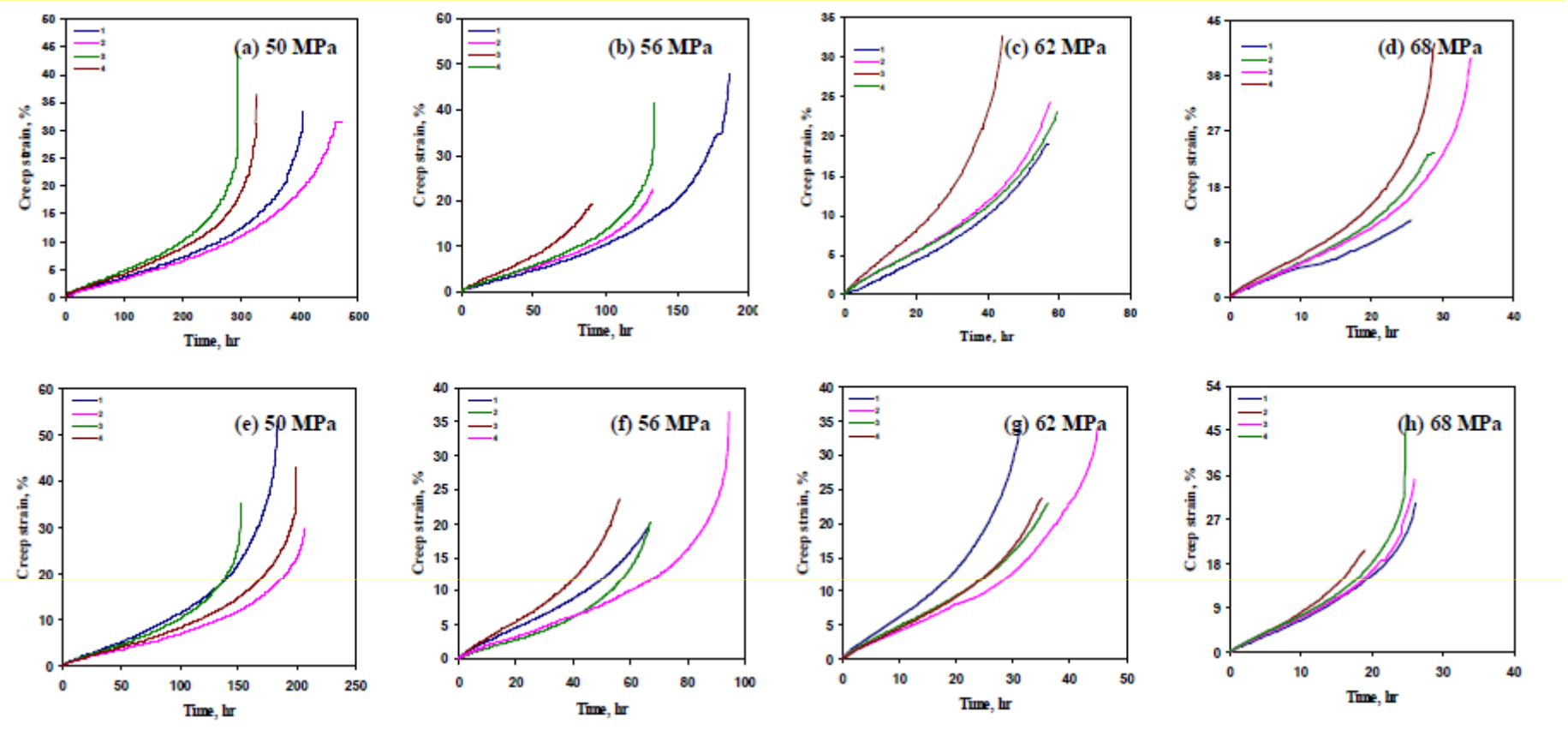


Fig 3 (a-d) Scatter creep curves at 870°C and at various stress levels of 11 years service exposed primary reformer tubes (top region) ; (e-h) Scatter creep curves at 870°C and at various stress levels of 11 years service exposed primary reformer tubes (bottom region).

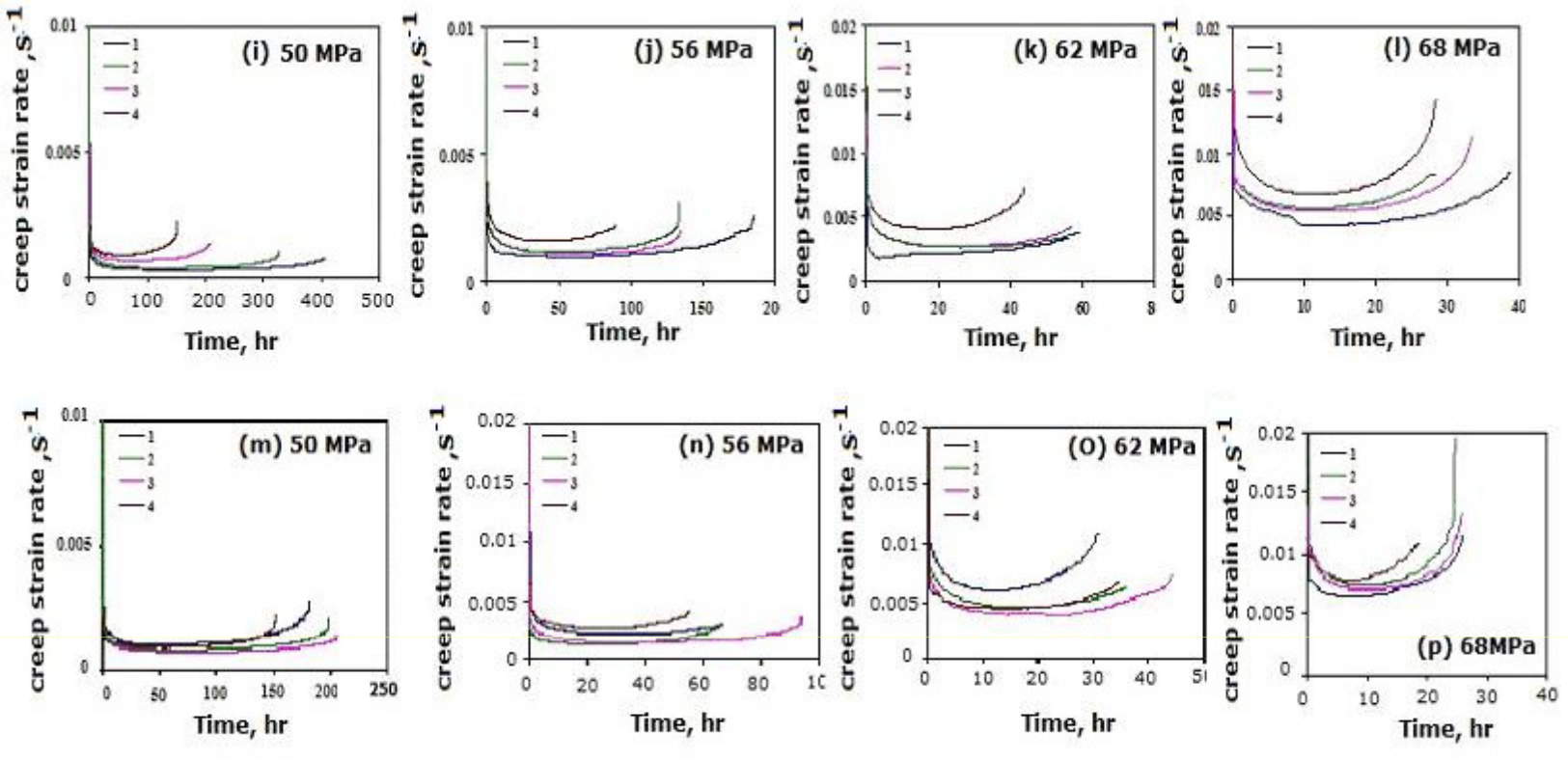
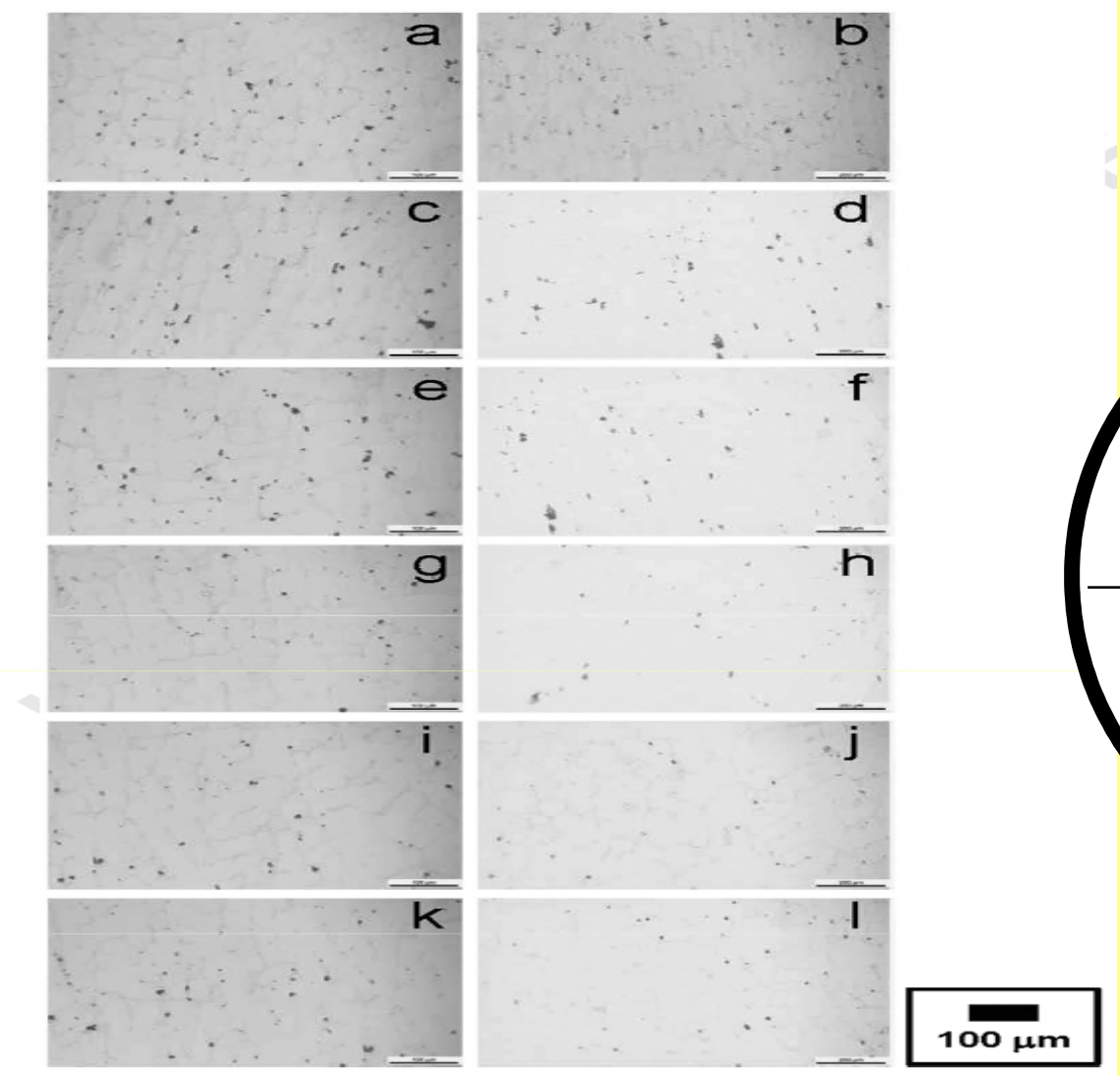


Fig 3 (i-l) Creep strain rate curves at 870° C and at various stress levels of 11 years service exposed primary reformer tubes (top region) ; (m-p) Creep strain rate curves at 870° C and at various stress levels of 11 years service exposed primary reformer tubes (bottom region).



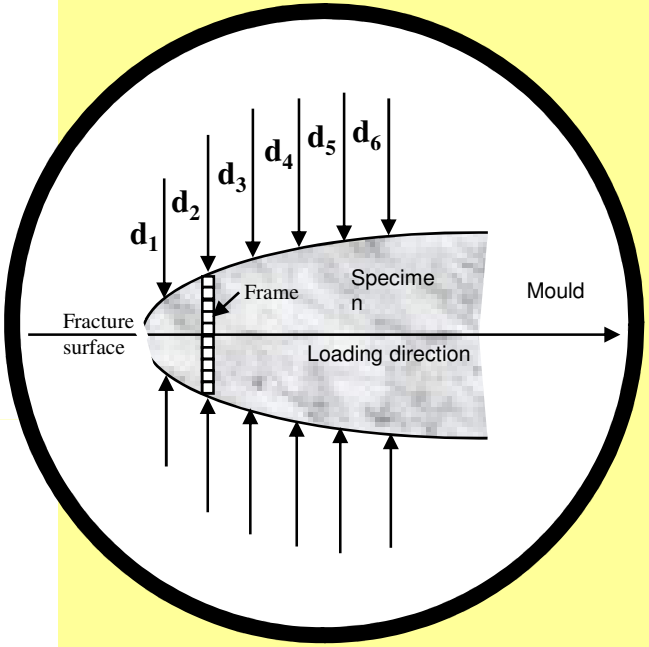
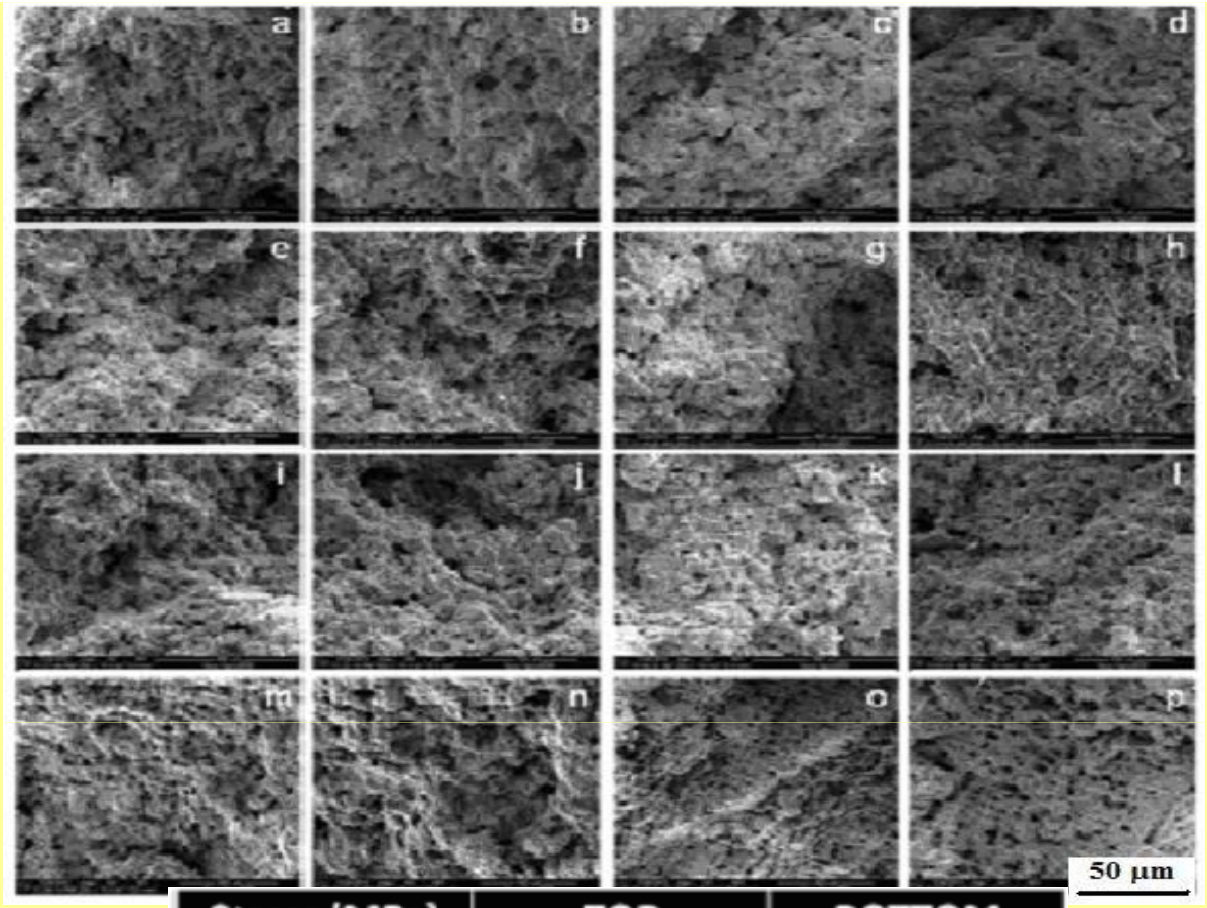


Fig.4a Typical representation of **creep cavitation of top** region at **50 Mpa** (a,c,e,g,i,k) and **68 MPa** (b,d,f,h,j,l) .True strain at (a) 1.187, (c)0.897, (e) 0.626, (g) 0.525, (i) 0.398, (k) 0.359, (b) 0.781, (d) 0.652, (f) 0.565, (h) 0.40, (j) 0.244 and (l) 0.149



Stress (MPa)	TOP	BOTTOM
50	a, b	c, d
56	e, f	g, h
62	i, j	k, l
68	m, n	o, p

Fig.4b Fractograph of crept service exposed specimens (both top and bottom portion of the tube) tested at **870 °C** in the stress range of **52-68 MPa**.

Deterministic Approach: CDM model for creep damage

The work of **Kachanov and Rabotnov** is of considerable relevance to evaluate material degradation due to creep. They assumed that during creep, **damage accumulation** progressively reduces the effective **load bearing cross sectional area** of a specimen from an **initially intact condition to a complete loss when rupture occurs**.

The **rate of strain accumulation** can be predicted throughout the creep life by introducing a generalized **damage parameter (ω).** Predictions of **damage or loss of continuity** are made possible by a set of two coupled equations which fit the limiting conditions i.e., **ω = 0** at time **t** = 0 and **ω = 1** at time **t** = t_r as

$$\frac{d\varepsilon}{dt} = \frac{A\sigma^n}{(1-\omega)^n} \qquad (2)$$

$$\frac{d\omega}{dt} = \frac{B\sigma^m}{(1-\omega)^\eta} \qquad (3)$$

A, B, n, m and η are material constants

Kachanov, L.M., 1958. Rupture time under creep conditions. Izv. ANSSSR. OTN 8, 26-31.

Rabotnov, Yu N., 1969. Creep Problems in Structural Members, North-Holand Publication Co., London.

Following **Cane** Eq.s (2,3) can be integrated for constant stress conditions to give

$$\omega = 1-(1-\frac{t}{t_r})^{\frac{1}{\lambda}} \qquad (4)$$

Where, **λ** is **creep damage tolerance factor** and is defined as the ratio of **strain to failure to the Monkman-Grant constant** i.e

$$\lambda = \varepsilon_r / \dot{\varepsilon}_m \, t_r$$

The product $\dot{\varepsilon}_m \, t_r \equiv \varepsilon_s$ is the Monkman-Grant constant. λ is a significant parameter in assessing the susceptibility of a material to localized cracking at strain concentrations and is also suggested as a better measure of creep ductility. Its value for engineering all ranges from 1 to about 20.

Cane, B.J., 1983. Estimating the remanent creep life of power plant components. High Temp. Technol.1, pp. 21

The A- parameter which is equated to the damage parameter, ω from K-model has been related to the measured parameter A_1 by following [x]as:

$$A = \omega = A_1 \times 4/\pi \quad (5)$$

where A_1 is number fraction of cavitated grain boundaries on the reference line.

Since quantification of voids in the present crept material has shown that the probability of number of creep cavities or voids at the GBTP (A_2) junctions along a reference line, is three times than that of the number of creep cavities or voids occurring along the GB (A_1) [y], a relation A_1 and A_2 can be obtained as:

$$A_2 = 3 A_1 = 3 A * \pi/4 \quad (6)$$

---

[x] Eggeler G, Brear JM, Cane BJ, Martinez-Ofia R, Baries Fernandez J, Borregan JM, Navarro A, In: Proc. 4th Int. Conf. on Creep and Fracture of Engineering Materials and Structures. University College, Swansea; 1990.

[y] Das A, Roy N and Ray AK, Stress induced creep cavity. Mater Sc. Engg A 2014; 598: 28–33.

Cavitated GB and GBTP counted for the determination of A_1 and A_2 parameters were measured according to Riedel [z].

GB and GBTP were considered to be damaged when it contained cavity of size greater than or equal to 1 μm. Using the

stereological results from Eggler et al. [x], A* is derived as the cumulative contribution from damaged grain boundaries (A_1) and number of creep cavities or voids at the grain boundary triple points (A_2). Therefore, we arrive at the following:

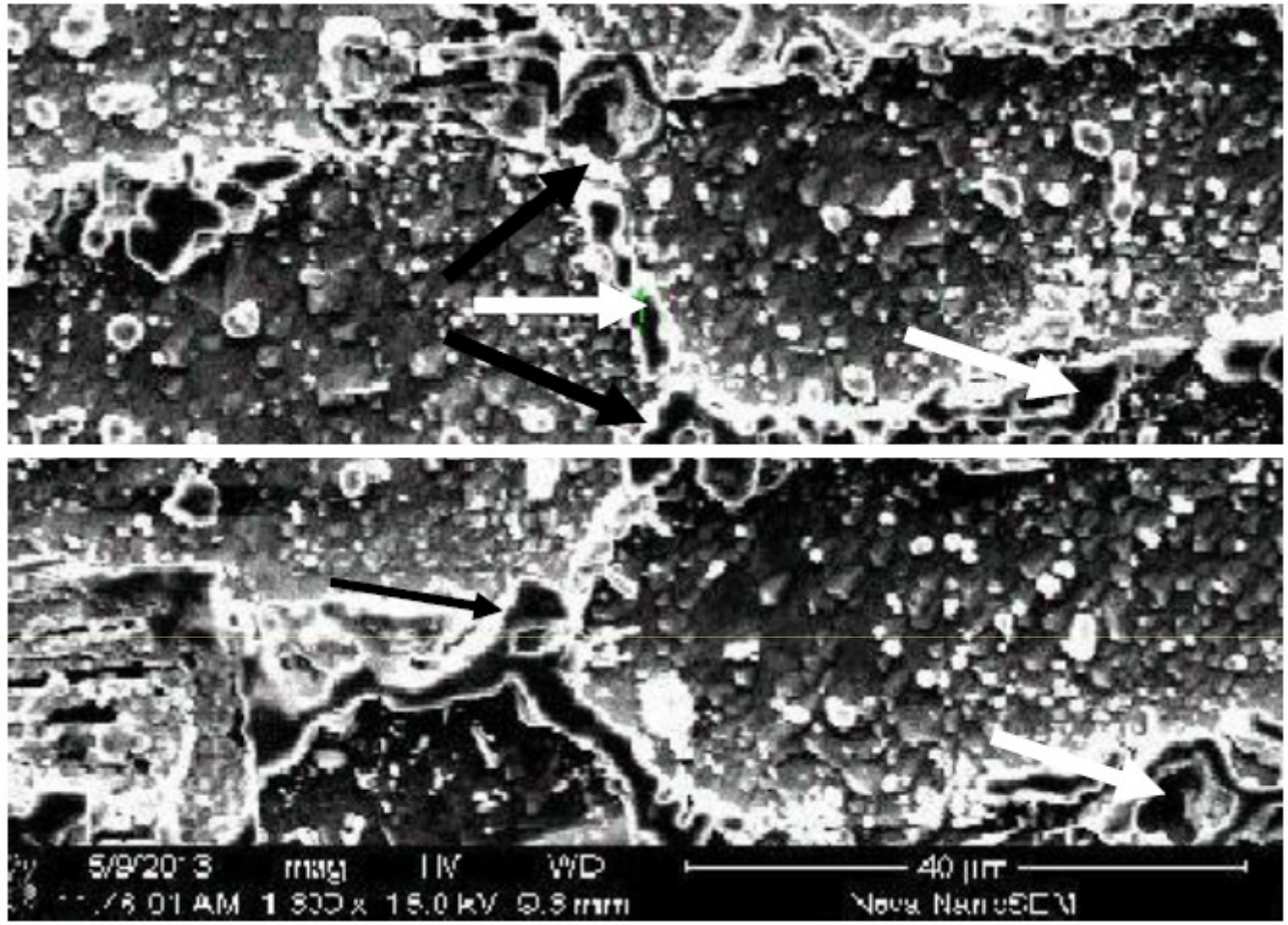
$$A^* = A_1 + A_2 = \pi A/4 + 3\pi A/4 = \pi A \qquad (7)$$

It is more appropriate if 3D measurements of creep cavitation could be carried out. However, due to experimental limitation 2D measurement was resorted to, extensively.

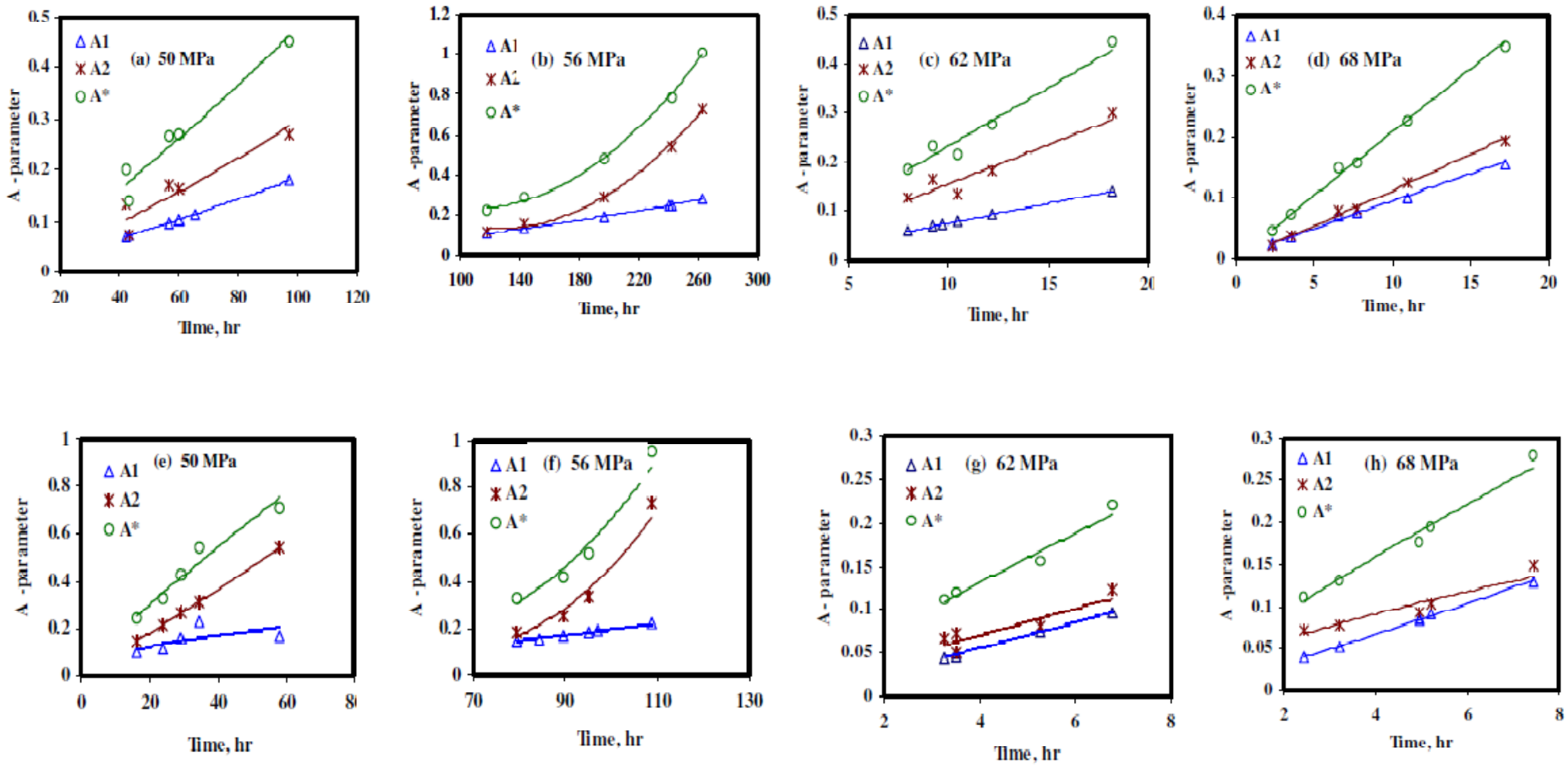
---

[x] Eggeler G, Brear JM, Cane BJ, Martinez-Ofia R, Baries Fernandez J, Borregan JM, Navarro A, In: Proc. 4th Int. Conf. on Creep and Fracture of Engineering Materials and Structures. University College, Swansea; 1990.

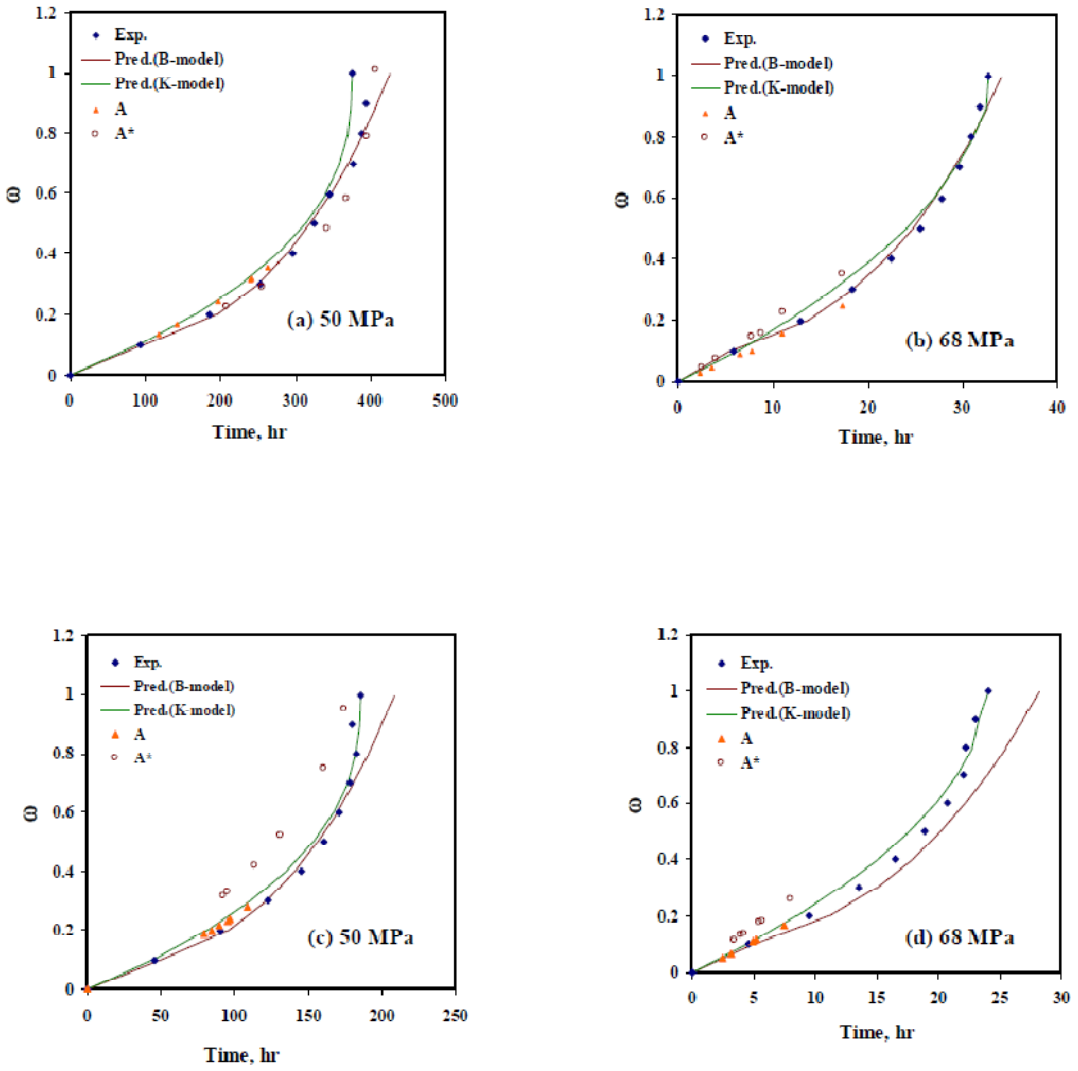
[z] Riedel H, Life prediction methods for constrained grain boundary cavitation. Int J Press Vess Piping 1989; 39:119-134.



SEM micrograph at 50 MPa/870°C, revealing creep cavitation/void formation at GB (white arrow) and at GBTP (black arrow) which were digitally recorded along a reference line indicated in white.



Comparison of microstructurally determined damage parameter **A1**, **A2** and **A***: (a-d) top and (e-h) bottom portion of service exposed reformer tube at 870 ^{o}C



Comparison of damage parameter A and A* with the damage prediction from probabilistic model as well as K-model at 870 °C: (a,b) top and (c,d) bottom portion of service exposed reformer tube.

The microstructurally quantified damage (creep cavitation /voids) is in close agreement with the damage prediction curves based on K-model as well as B-model, at low stress (50 MPa) where as at high stress (68 MPa) it could correlate well till the mid region of the predicted curves, above which cavity measurement was practically not feasible . This is because at high temperature and at high stresses grain boundary sliding occurs discontinuously with time and amount of shear displacement is not uniform in the adjacent grains.

But grain boundary at high temperature and high stresses can be accommodated by formation of folds at the grain boundaries [R]. When distribution of shear stress is non uniform amongst the adjacent grains, at high stresses these folds may not be apparent as clear voids and possibly due to this fact void quantification under light optical microscope and SEM was only possible till the mid portion of the predicted curves.

It is observed that the A* is more sensitive to life prediction than A because it picks up the localized damage in the form of voids which actually forms in the tertiary region of creep life.

[R] Dieter GE, Mechanical Metallurgy, SI Metric ed. London : McGraw-Hill; 1988.

Stochastic Approach: Markov process for creep damage

Nucleation of cavities is one of the principal mechanisms of damage. It considers growth as nucleation on the interface between a **pre-existing cavity and the matrix**. With creep damage accumulation the distance between cavities keep decreasing and ultimately some of these may join together to produce a **microcrack**. This happens as and when a cavity nucleates in between two adjacent cavities.

The process continues leading to the **formation of macrocracks**. Ultimately the component fails as and when its load bearing cross section area is full of **cavities/cracks**. In fact **Fig. 1** gives a schematic representation of the above stages of nucleation and joining of cavities leading to fracture at different levels of strain accumulation. **A virgin material passes through each of these stages before failure occurs.**

The accumulation of **microcracks inside the material** is considered as a **cumulative damage process**. The process of damage accumulation during creep depends only on **its current state**. Therefore it is possible to simulate this by a **Markov chain process**:

$$\text{Prob}[S_{n+1} = j \mid S_n = i, S_{n-1} = k, \ldots, S_o = l] = \text{Prob}[S_{n+1} = j \mid S_n = i] \quad (5)$$

The indices **i, j, k**, etc. stand for the state number and S_n stands for **n**th event.

Eq. (5) says that **probability of S_{n+1}** being in state **j** is only **affected by the value of S_n** and the history of state value has no effect on S_{n+1}.

The **damage** is indexed by a finite set of states **1, 2, ..., *b***. State **1** means the **initial state with no damage** and state **b** means the **final damage state, i.e. failure or replacement**. The initial distribution of the different damage levels at time t = 0 may be defined by a **(1 x b)** row vector $\mathbf{p_o}$ as

$\mathbf{p_o} = \{ \pi_1, \ldots\ldots, \pi_b \}$ and $\sum_{j=1}^{b} \pi_j = 1$ (6)

The process of **cavitation is irreversible**. It can not heal. This means if it is in state S_i it can not move to S_j where **j < i**. Similarly even though the process of **damage accumulation during creep is discrete** it can not **bypass a particular state.**

This means a **virgin material before failure** must pass through each of the successive steps from **1** to **b**. So if a material is in state **1** now it can either remain in its present state or move to state **2**. Its probability of moving to state **3** and beyond is zero.

With these constraints the **transition matrix representing creep damage accumulation in a material** becomes as follows:

$$P = \begin{bmatrix} p_1 & q_1 & 0 & 0..... & 0 & 0 \\ 0 & p_2 & q_2 & 0..... & 0 & 0 \\ ..... & .....\ldots & .... & ..... & ..... & ..... \\ ..... & .....\ldots & ..... & ..... & ..... & 0 \\ & & & & & ..... \\ 0 & 0 & 0 & ..... & p_{b-1} & q_{b-1} \\ 0 & 0 & 0 & ..... & 0 & 1 \end{bmatrix} \qquad (7)$$

This **transition matrix P** describes that all states are transient, except for state **b** which is absorbing. According to **Markov process** this matrix can now be used to predict the state of the material after n^{th} step or during n^{th} **inspection interval** as

$$P_n = p_o P^n, \qquad n = 0, 1, 2, \ldots \tag{8}$$

To determine the **probability transition matrix P**, we introduce a random variable **W** in which $W_{1,b}$ denotes the **time to failure at state b** given that the process **starts in state 1**.

The mean and the variance of $W_{1,b}$ are

$$E\{W_{1,b}\} = (b-1) + \sum_{j=1}^{b-1} r_j \tag{9}$$

$$Var\{W_{1,b}\} = \sum_{j=1}^{b-1} r_j (1 + r_j)$$

$$r_j = \frac{p_j}{q_j}$$

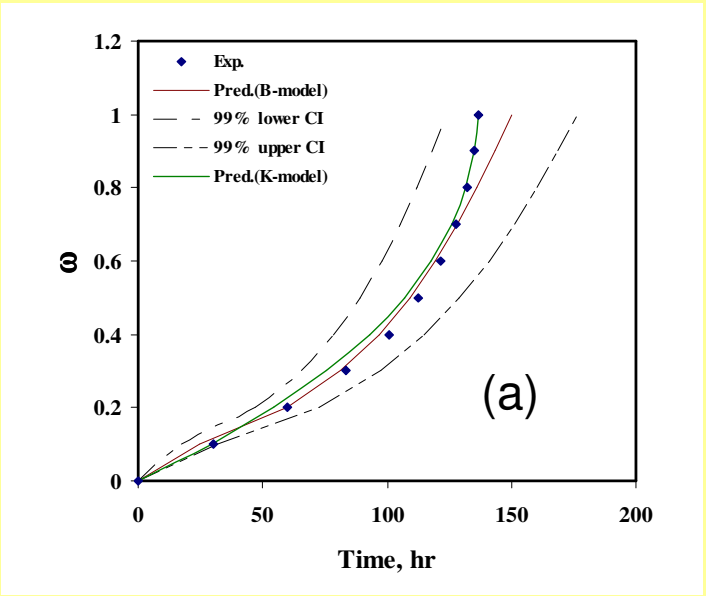
Statistical analysis of creep cavity area

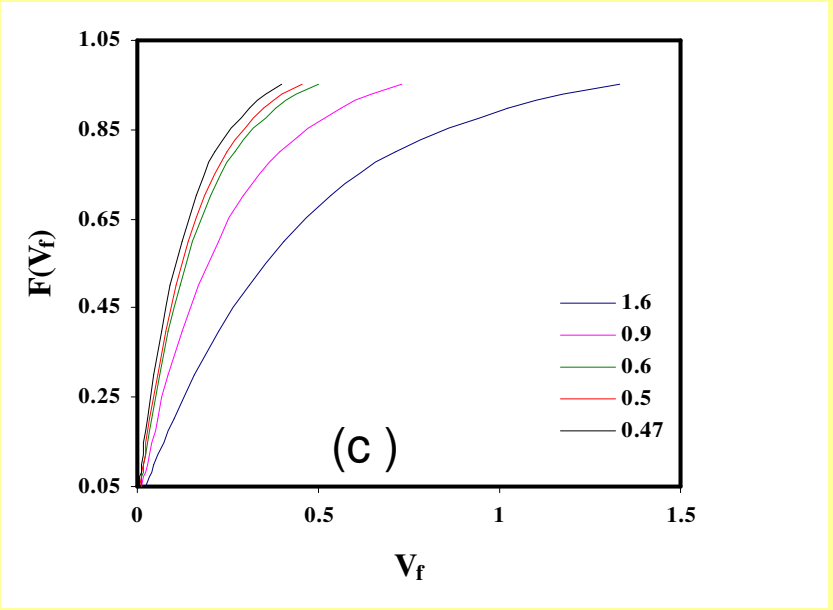
Nucleation of cavity is a **random process** and is strongly dependent upon the local stress-state and strain-state. It has been observed that over various test conditions, for the both top and bottom portion of the reformer tube the **normalised creep cavity area fraction** $\left(\frac{v_f}{\varepsilon}\right)$ follows the **Weibull distribution**.

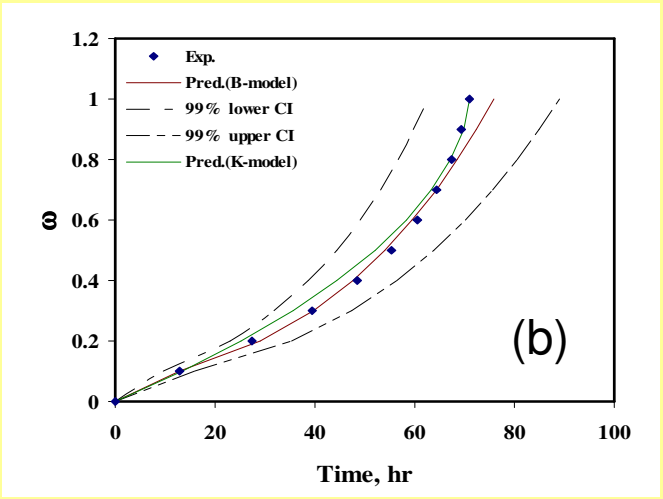
In terms of **true strain** (ε) and cumulative **probability of failure** P_f , creep **cavity area fraction** (v_f) can be probabilistically estimated as:

$$v_f = a\varepsilon\left(\left(-\ln(1-P_f)\right)\right)^{\frac{1}{b}} \qquad (10)$$

where **a** and **b** are Weibull parameter.







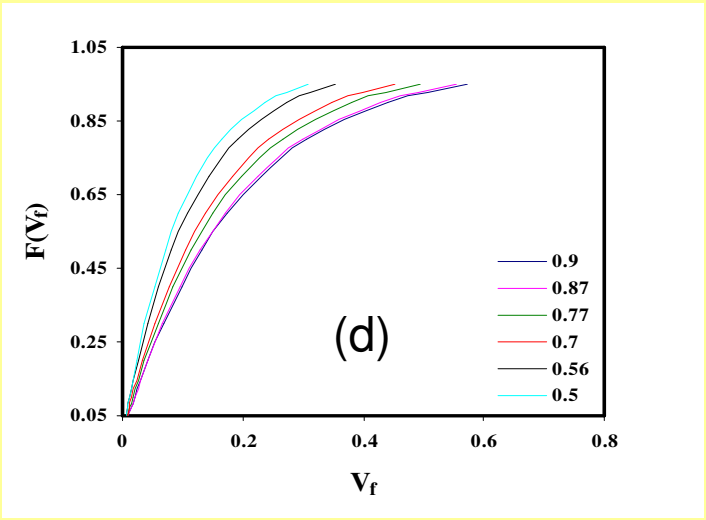
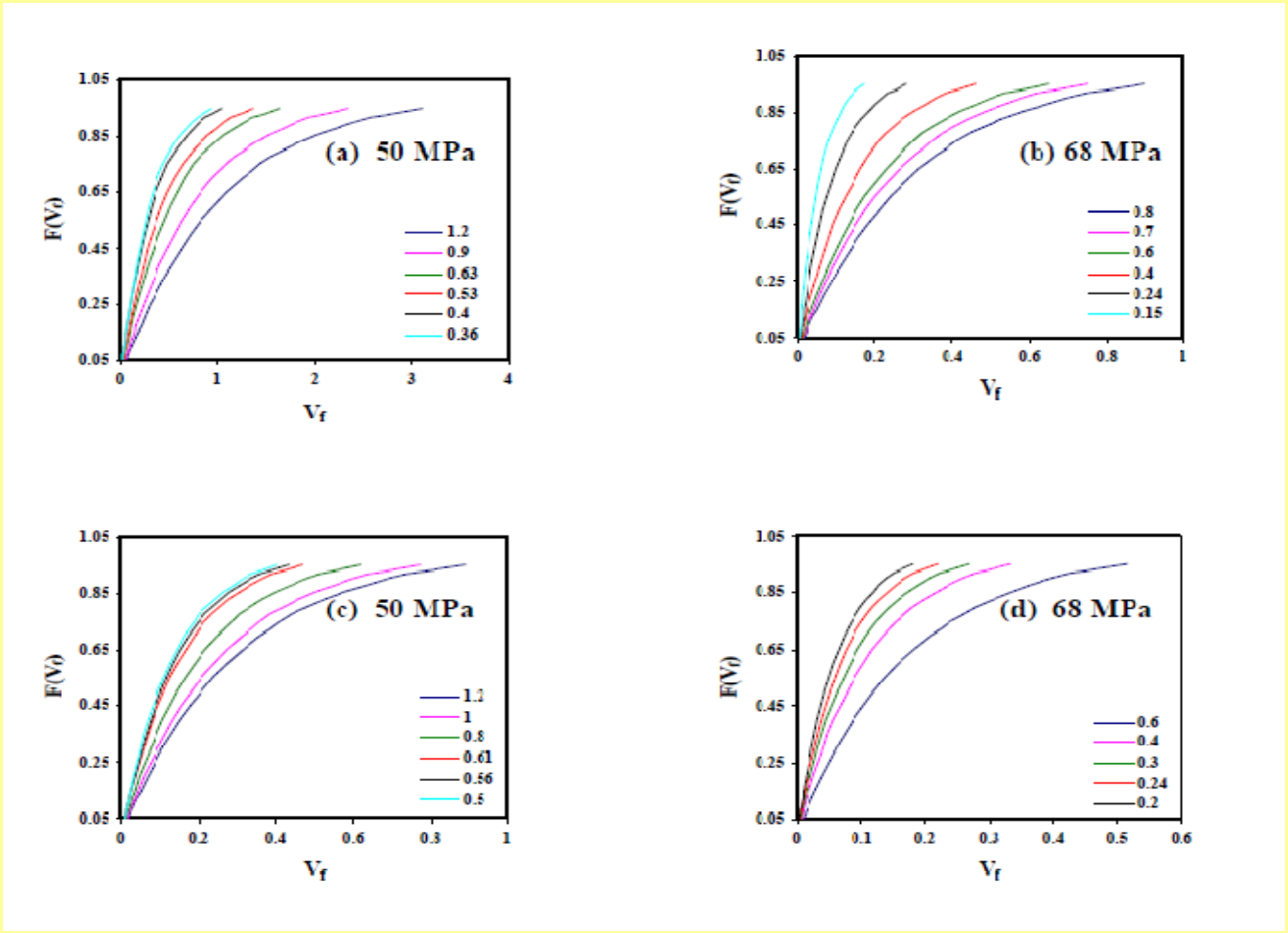


Fig.5 Comparison of the experimental and predicted values of mean time to reach a specified damage state by both Bogdanoff model and CDM approach with relative confidence interval (CI): (a) top and (b) bottom. Probability distribution of void area fraction: (c) top and (d) bottom portion of service exposed reformer tube at 870 °C/56 MPa.



Probability distribution of void area fraction at various true strain: (a,b) top and (c,d) bottom portion of service exposed reformer tube corresponding to 870 °C (stresses indicated).

Arpan Das , Nilima Roy and Ashok Kumar Ray, Stress induced creep cavity, Mater. Sc. and Engg A 598 (2014) 28–33

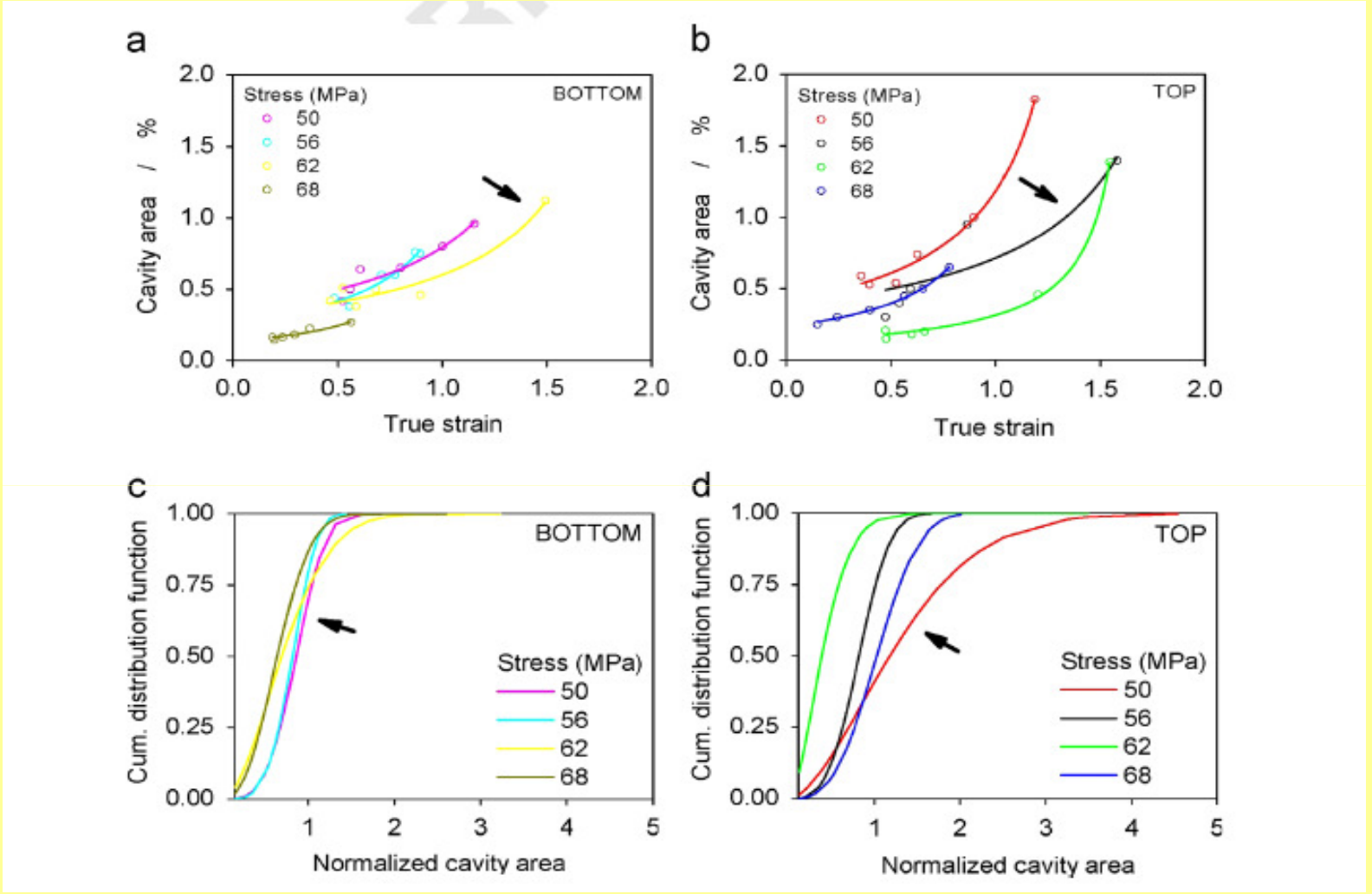


Fig.6 Cavity area as a function of strain for different stress levels for (a) **bottom** and (b) **top** tubes. **Cumulative distribution functions** as a function of **normalised cavity area** (cavity area/true strain) for (c) bottom and (d) top tubes.

Arpan Das , Nilima Roy and Ashok Kumar Ray, Stress induced creep cavity, Mater. Sc. and Engg A 598 (2014) 28–33

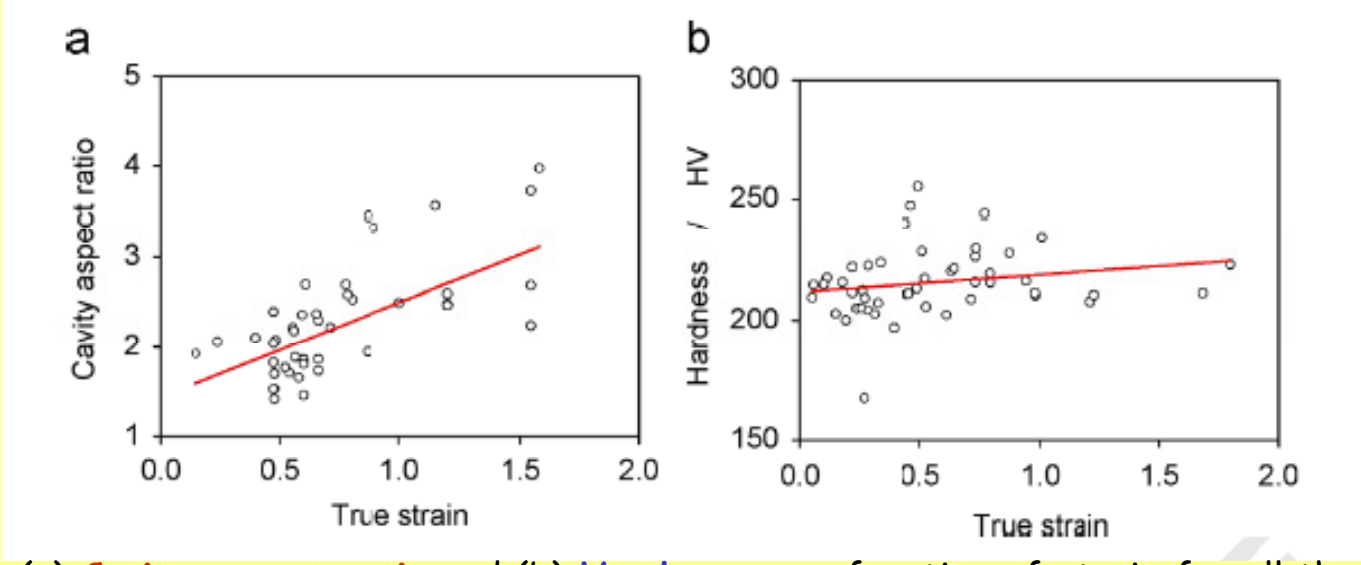


Fig.7 (a) **Cavity aspect ratio** and (b) **Hardness** as a function of strain for all the stress levels for both top and bottom tubes together.

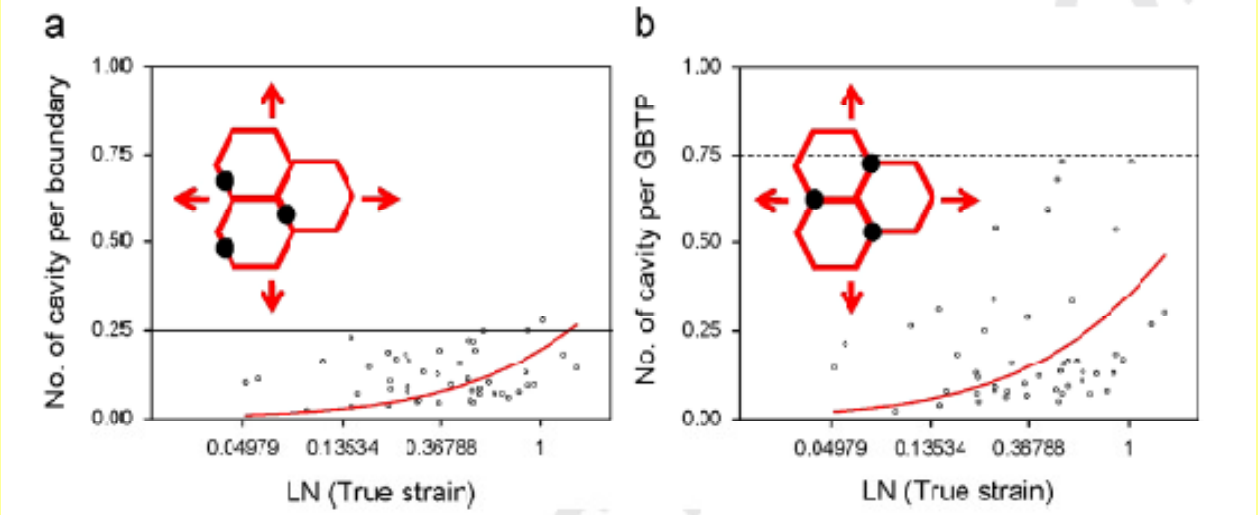
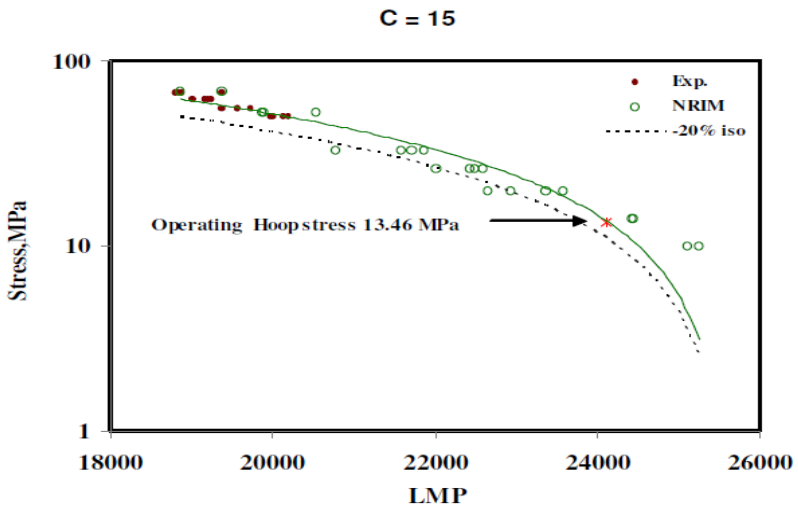
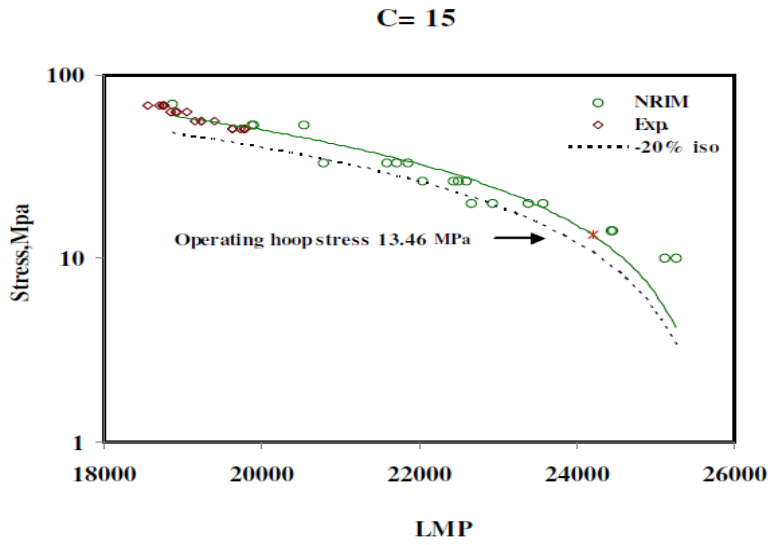


Fig.8 (a) Number of **creep cavity formation at GB** and at (b) **GBTP** as a function of strain for all stress levels for both the top and bottom tubes together.



(a)



(b)

Stress vs LMP Plot for 11 years service exposed Reformer tube materials (a) top and (b) bottom for comparison with –20% NRIM standard data line. All data fall on the NRIM virgin data line

Table . 1 Remaining life at different temperature with varying C (LMP constant) value

Component (service exposed)	Hoop Stress, MPa	Temp	C (LMP constant)	LMP of Service exposed material	Life (t_r), yrs	Remaining Life (RL)*, yrs
Reformer tube (Top)	13.46	870	20	30800	> 10	> 10
			15	24100	> 10	> 10
		920	20	30800	> 10	> 10
			15	24100	18	7
Reformer tube (Bottom)		870	20	30600	> 10	> 10
			15	24100	> 10	> 10
		920	20	30600	> 10	> 10
			15	24050	17	6

*** RL = t_r – 11 (service exposure in yrs)**

Conclusions

- **It appears that there is a systematic correlation of the creep cavitations and the applied stress at GB (grain boundaries) and GBTP grain boundary triple point). The probability of GBTP cavitations is more than that of GB cavitations where the initial inclusion volume fraction/ other second phase particles for all the specimens were kept constant.**

- **The present investigation concludes that cavity nucleation occurs at lower strain at higher stressed specimens and vice versa. The early cavity nucleation takes place at higher stress and vice versa.**

Arpan Das , Nilima Roy and Ashok Kumar Ray, Stress induced creep cavity, Mater. Sc. and Engg A 598 (2014) 28–33

- The inhomogeneous distributions of GB and GBTP in the deformed austenite dendrites help nucleate the cavity, which grows under the influence of favourable plastic strain and hydrostatic stress and then coalescences where the initial inclusion content and other second phase particles were kept unaltered.

Arpan Das , Nilima Roy and Ashok Kumar Ray, Stress induced creep cavity, Mater. Sc. and Engg A 598 (2014) 28–33

- For the same amount of true strain, the creep cavity area was found to be higher for the low stress specimen than that of the high stress. Also, to reach the same amount of cavity area fraction, the higher stress specimen needs a higher amount of accumulated strain than the lower stress for both the top and bottom portion of the tube.

[Arpan Das , Nilima Roy and Ashok Kumar Ray, Stress induced creep cavity, Mater. Sc. and Engg A 598 (2014) 28–33]

- Considerable amount of scatter was observed in creep deformation and creep strain rate curve at 870°C of service exposed material of both top as well as bottom portion of the reformer tube at various stress conditions. Although there was evidence of ductile dimples in top as well as bottom portion of the tube, mode of fracture mainly varied from ductile-quasi cleavage-brittle failure. This was probably responsible for experimental scatter.

Arpan Das , Nilima Roy and Ashok Kumar Ray, Stress induced creep cavity, Mater. Sc. and Engg A 598 (2014) 28–33

- The prediction of mean time to reach a specific damage state from proposed probabilistic model is in close agreement with that of CDM model and can describe the abrupt changes of the creep damage in the tertiary region as well. The probability of failure due to creep cavity area at various true strain follows Weibull distribution. The distribution shifts towards the higher range of creep cavity with increase in strain.

•From statistical point of view, the pattern of Weibull distribution followed for analyzing probability of rupture due to cavity or void area, shifts with increase in true strain towards the higher population of void.

•Experimental data for estimating damage in the material, agrees well with simulation based CDM (continuum damage mechanics) model as well as B-model for prediction of damage with scatter associated with it. In other words, estimation of average time to reach a specific damage state from both the models are in close agreement with that of experimental data. This pertains to the sudden changes in creep damage in the tertiary region.

•The microstrucrally determined damage parameters A and A* are compared with the damage prediction by the probabilistic model. The prediction could correlate till the mid region of the curves at high stress where cavity measurement was practically feasible. It is observed that the A* is more sensitive to life prediction than A because it picks up the localized damage in the form of voids which actually forms in the tertiary region of creep life.

•An additional life of 〉 10 years is predicted at the operating stress–temperature conditions of the top as well as bottom portion of the service exposed primary reformer tube

•At the design temperature of 920°C/13.46 MPa an additional minimum balance life of 7 years and 6 years for the top and bottom portions of the 11 years service exposed primary reformer tubes respectively is possible, provided there is no evidence of any localised damage in the form of surface cracks, cavitation or dents and overheating of the tubes resulting in early onset of creep damage. Another check for safety of the service exposed tubes, similar to the current work, in terms of residual life is recommended to be carried out after expiry of about 2.5 years of service life from the view of economical and safety reasons. Also during shut down of the plant, NDT (nondestructive) tests viz. Dimensional (thickness and diameter) measurement, hardness measurement and in situ metallography may be carried out to assess the condition of the materials for their future serviceability.

Part II:

Case Study 2

Microstructural studies and remnant life assessment of eleven years service exposed reformer tube

Ashok Kumar Ray, Sudheer Kumar, Guguloth Krishna, Manoj Gunjan, B. Goswami, Samir Chandra Bose

Materials Science and Engineering A 529 (2011) 102– 112

Table.1: Operating parameters and service history of the primary reformer

Reformer box dimensions (each Chamber)	Length : 39490 mm Width : 2611990 mm Height : 11990 mm
Pressure inside the reformer tubes	32 Kg/cm^2
Fuels used for main burners	Natural gas
General expected gas composition inside the reformer box	CO :Nil;,CO_2 :9.12 %, SO_2: Nil, $NO_{2:}$:3.2 ppm, H_2 :Nil, N_2 : 70.96%; O_2 :0.96% :
Reformer tube material	KHR 35 CT (25 Cr / 35 Ni / 1.0 Nb / 0.5 Ti max/ 0.03 Mo)
Reformer tube diameter	O.D.(outer diameter): 152 mm I.D (inner diameter). : 129 mm
Reformer tube thickness	11.5 mm
Reformer tube recommended design skin temperature	950 ^oC
Reformer tube inside temperature	Tube inlet temp. : 494 ^oC Tube exit temp. : 763 ^oC
Present method of reformer tube skin temperature measurement	By infrared pyrometer; Model : Cyclops 339
Previous shut down of the plant	September 2005

Table2: Chemical analysis of the service exposed primary reformer tubes

Sl. No	Material type	Wt % of Elements present								
		C	Ni	Cr	Nb	Ti	Mn	P	S	Mo
1.	Tube no 103, primary reformer	0.47	34.9	24.75	0.97	0.2	0.97	0.010	0.005	0.01
2.	Tube no 141, primary reformer	0.43	35.2	25.44	1.03	0.3	1.01	0.012	0.009	0.015
3.	KHR 35 CT	0.48	35	25	1.0	0.5	1.02	0.014	0.009	0.03

Materials Science and Engineering A 529 (2011) 102– 112

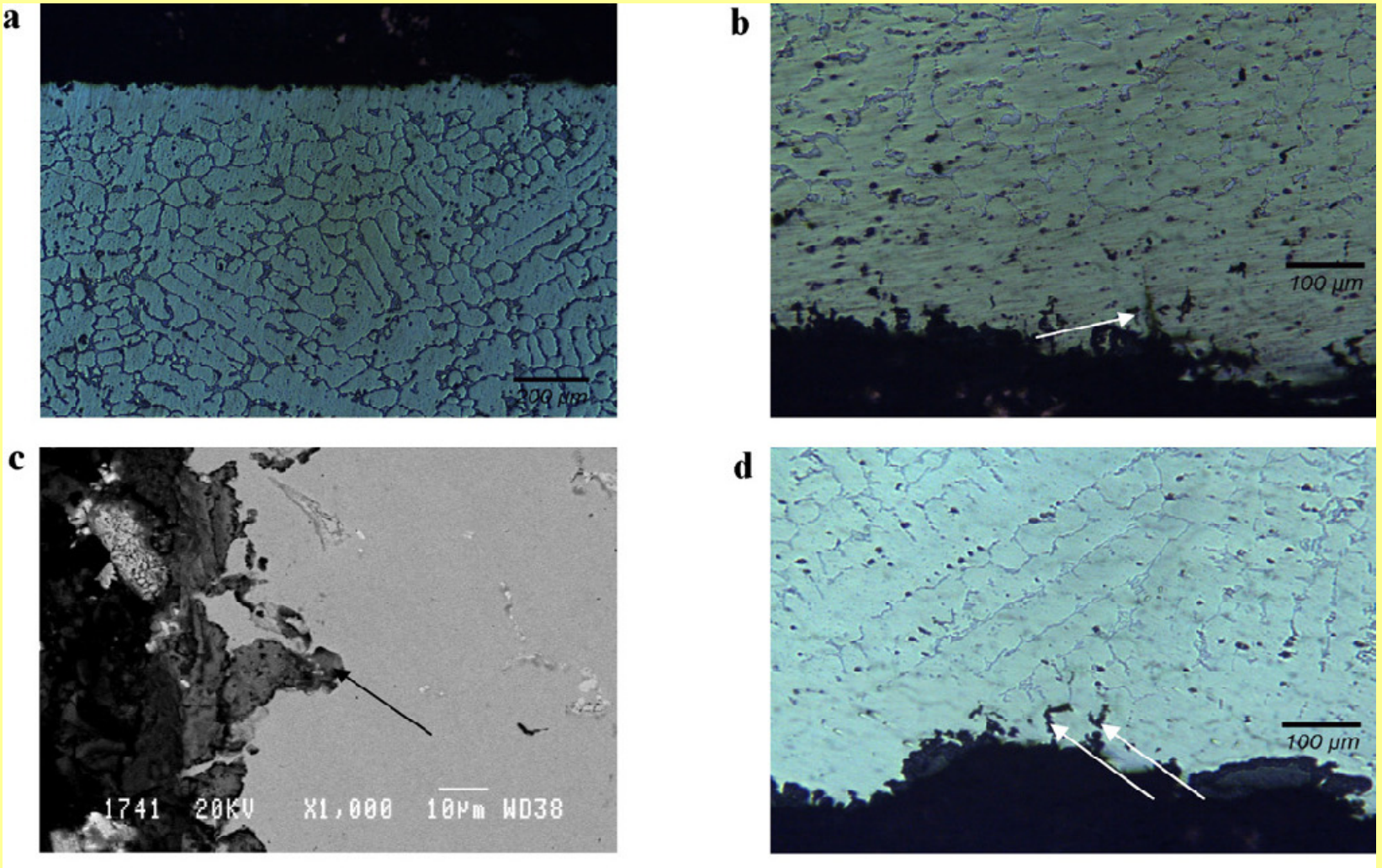
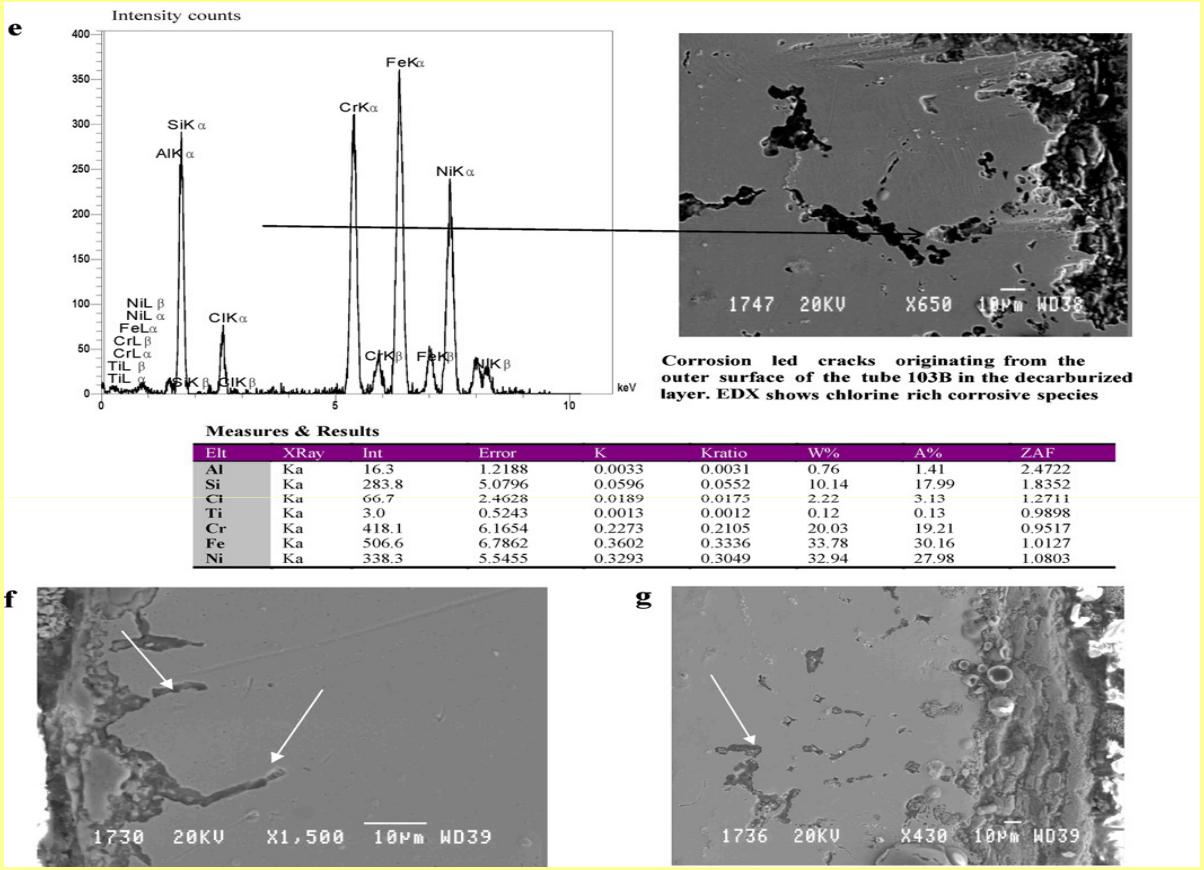


Fig. 1. (a) Optical microstructure of tube no 103B showing decarburization at inside edge and dendritic matrix, 50×. (b) Optical microstructure of tube no 141B showingdecarburization and corrosion attack at inner surface of the tube, 100×. (c) SEM image of tube no 103B showing decarburization and corrosion attack at internal surface as shown by an arrow. (d) Optical metallograph of inner surface of service exposed tube no 141 M revealing decarburization and presence of corrosion cracks along theinter-dendritic boundaries indicated by arrow. The structure is basically columnar type.

Materials Science and Engineering A 529 (2011) 102– 112



Measures & Results

Elt	XRay	Int	Error	K	Kratio	W%	A%	ZAF
Al	Ka	16.3	1.2188	0.0033	0.0031	0.76	1.41	2.4722
Si	Ka	283.8	5.0796	0.0596	0.0552	10.14	17.99	1.8352
Cl	Ka	66.7	2.4628	0.0189	0.0175	2.22	3.13	1.2711
Ti	Ka	3.0	0.5243	0.0013	0.0012	0.12	0.13	0.9898
Cr	Ka	418.1	6.1654	0.2273	0.2105	20.03	19.21	0.9517
Fe	Ka	506.6	6.7862	0.3602	0.3336	33.78	30.16	1.0127
Ni	Ka	338.3	5.5455	0.3293	0.3049	32.94	27.98	1.0803

Fig.1(e) SEM image of tube no 103B showing immense corrosion attack, as shown by an arrow, at the outer surface of the tube.
(f) SEM image of tube no 141B showing decarburization and corrosion attack, as shown by an arrow, at the inner surface of the tube.
Fig.1 (g) SEM image of tube no 141B showing decarburized and corroded outer surface (arrow shows the attack).

Materials Science and Engineering A 529 (2011) 102– 112

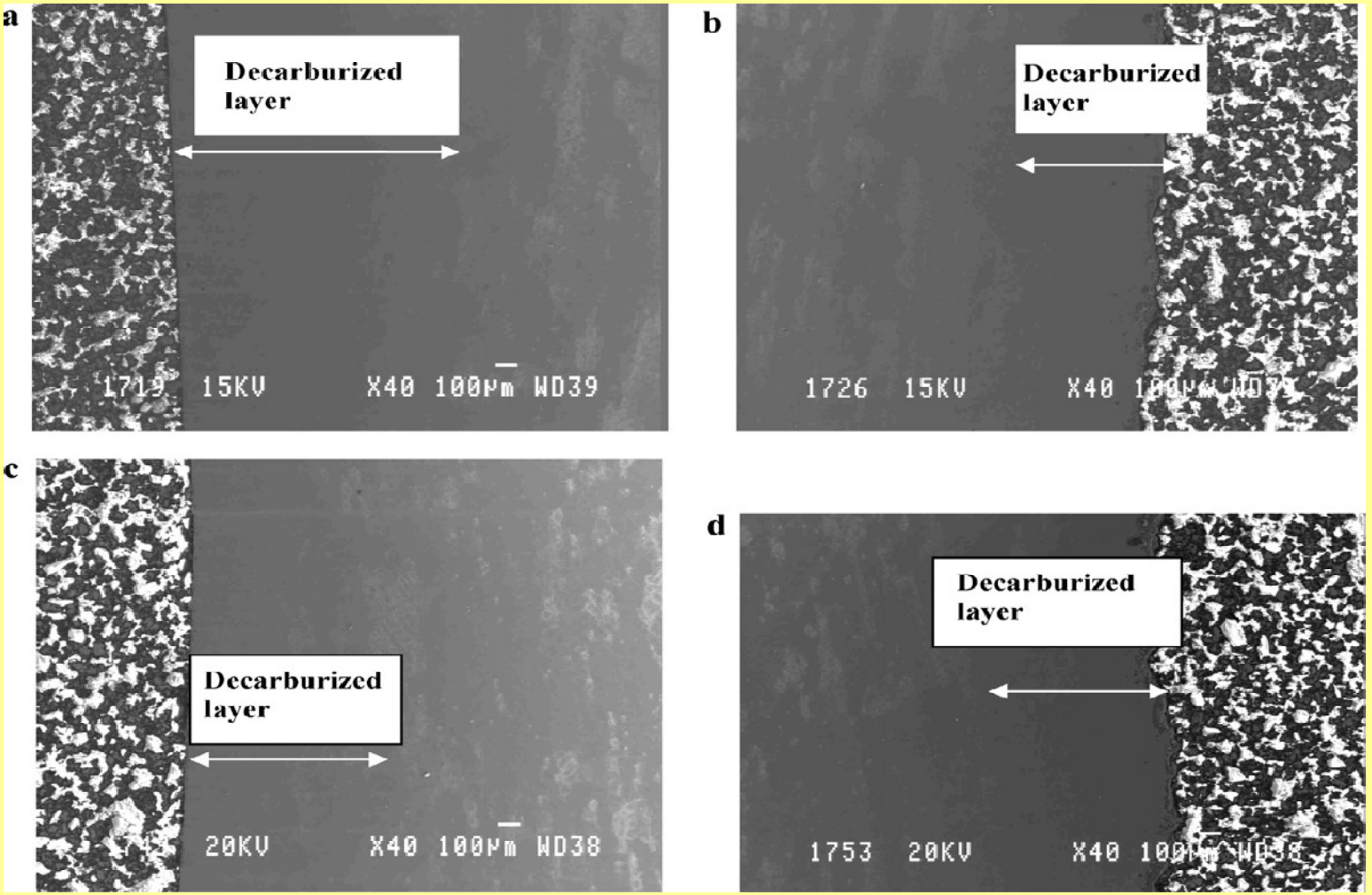


Fig. 2. (a) SEM image of tube no 103M showing mainly decarburized layer at inner surface. (b) SEM image of tube no 103M showing decarburized layer at the outer surfaceof the tube. (c) SEM image of tube no 141M showing decarburized internal surface. (d) SEM image of tube no 141M showing decarburized layer at the outer surface.

Materials Science and Engineering A 529 (2011) 102– 112

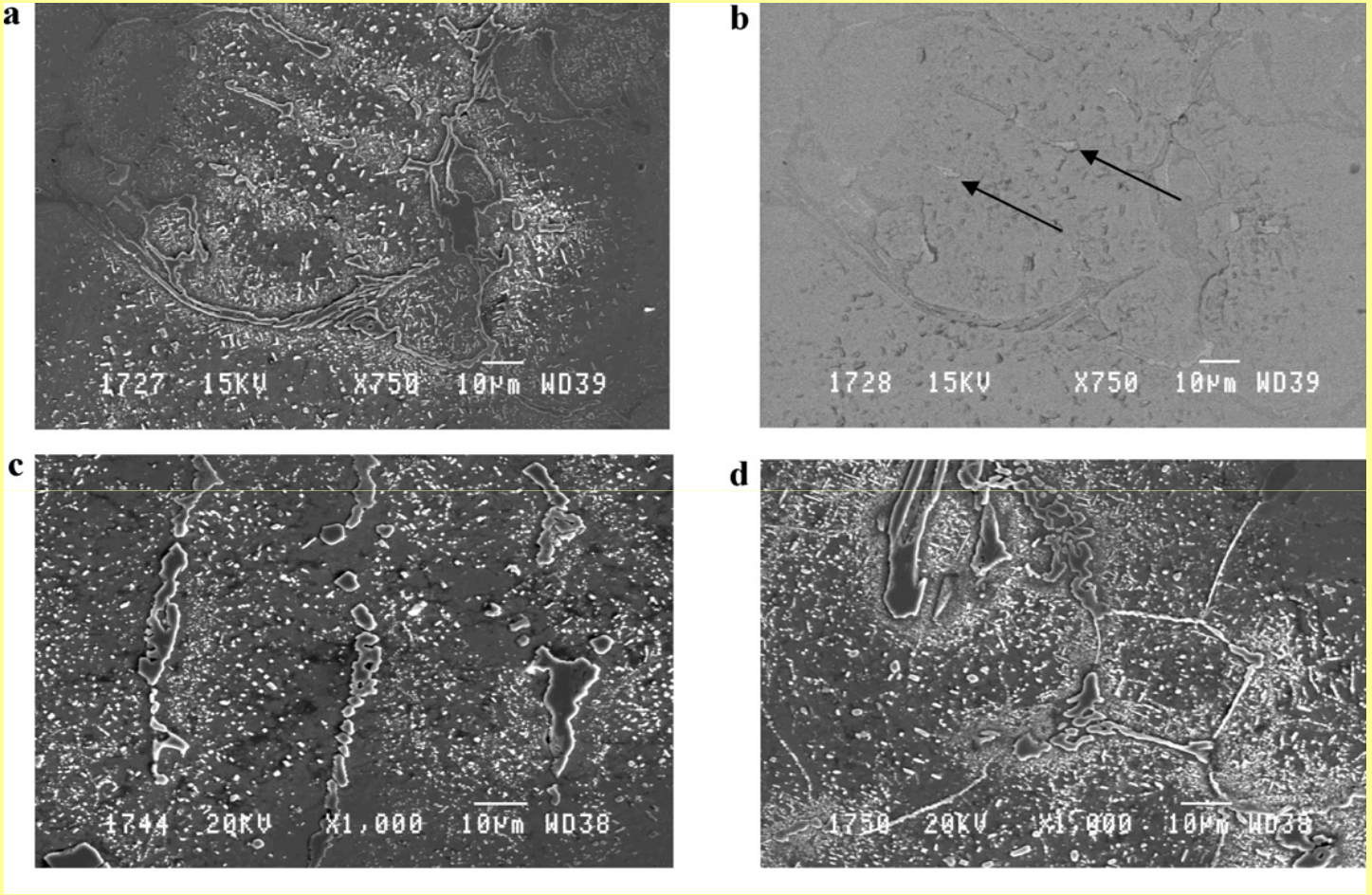


Fig. 3. (a) SEM image of the outer surface of tube 103M, revealing coarse $M_{23}C_6$ carbides at dendritic boundaries and massive secondary precipitation of Cr and Nb rich intra-dendritic carbides. The dendritic carbides are mostly Cr rich. (b) Back scattered image of the above figure showing localised accumulation of Nb-rich carbides indicated by arrow. (c) SEM image of tube no 103B showing the coarse $M_{23}C_6$ carbides at dendritic boundaries and secondary fine precipitations within dendrites. No creep cavities are revealed. (d) SEM image of service exposed tube no 141 M at mid section.

Materials Science and Engineering A 529 (2011) 102– 112

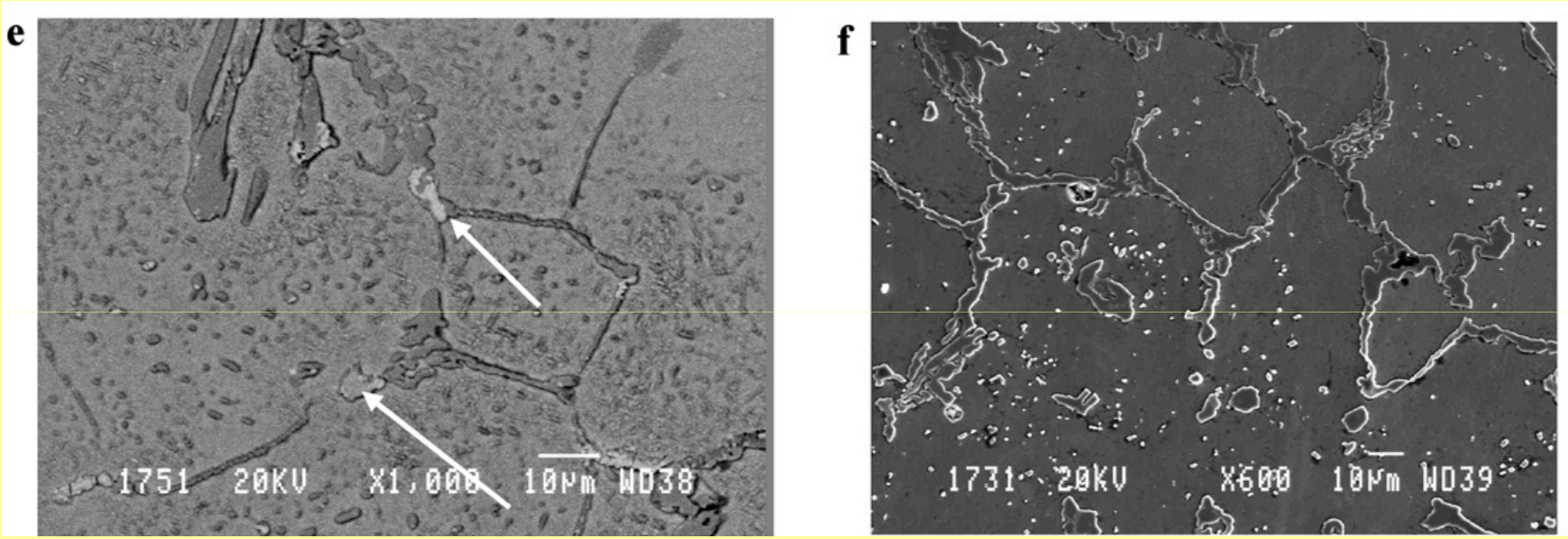
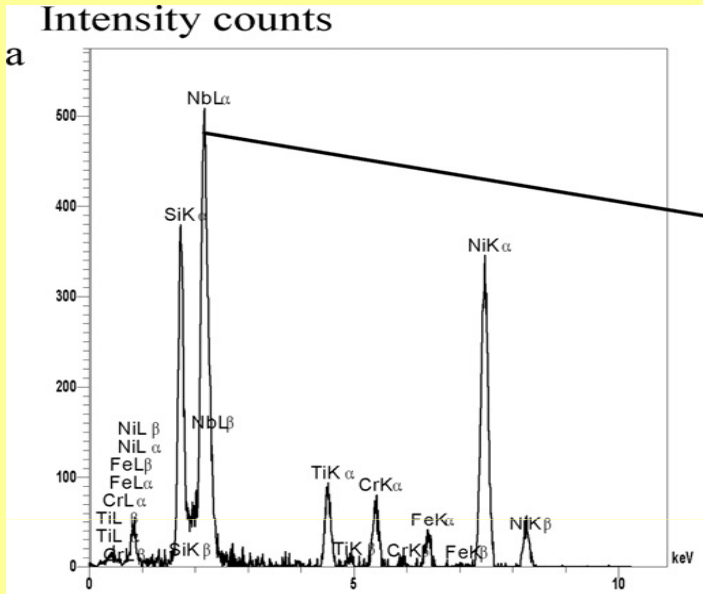
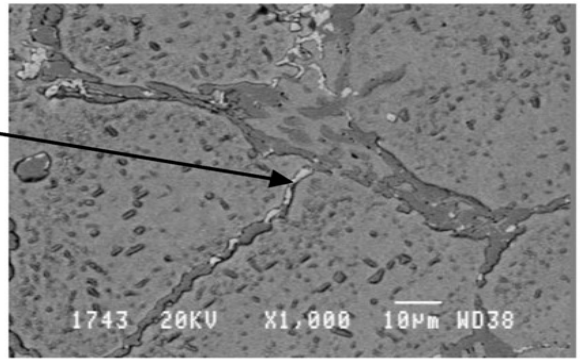


Fig.3(e) back scattered image of (d) showing the Nb rich phases at preferable locations indicated by arrows. (f) SEM image of 141B showing the coarse carbides at dendritic boundaries and disappearance of fine intra dendritic precipitation. It appears that tube might have over heated. There is no creep cavitation or voids seen.

Materials Science and Engineering A 529 (2011) 102– 112



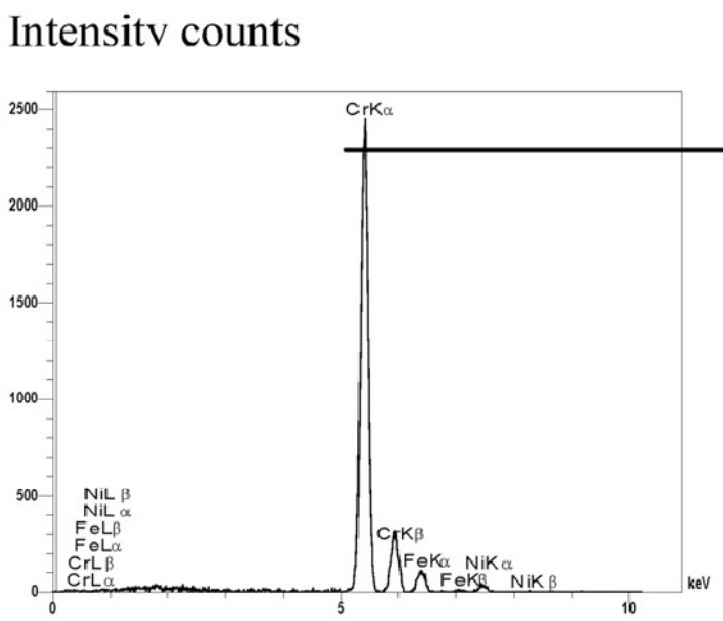


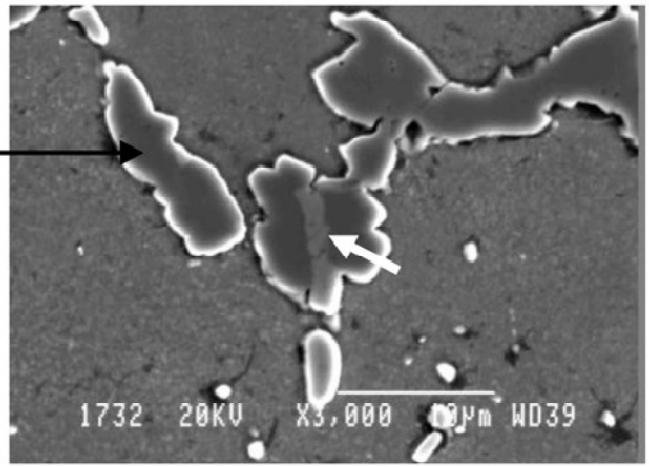
Back scattered image of primary dendritic boundary carbide (fair) showing preferential accumulation of Nb in tube 141B

Measures & Results

Elt	XRay	Int	Error	K	Kratio	W%	A%	ZAF
Si	Ka	144.0	2.1553	0.0969	0.0824	13.39	26.52	1.6239
Ti	Ka	37.3	1.0964	0.0518	0.0440	4.80	5.58	1.0899
Cr	Ka	29.9	0.9826	0.0521	0.0443	4.54	4.86	1.0250
Fe	Ka	14.7	0.6878	0.0334	0.0284	2.71	2.70	0.9537
Ni	Ka	167.8	2.3268	0.5231	0.4451	45.03	42.67	1.0118
Nb	La	182.8	2.4286	0.2427	0.2065	29.52	17.68	1.4296
				1.0000	0.8508	100.00	100.00	

Materials Science and Engineering A 529 (2011) 102– 112





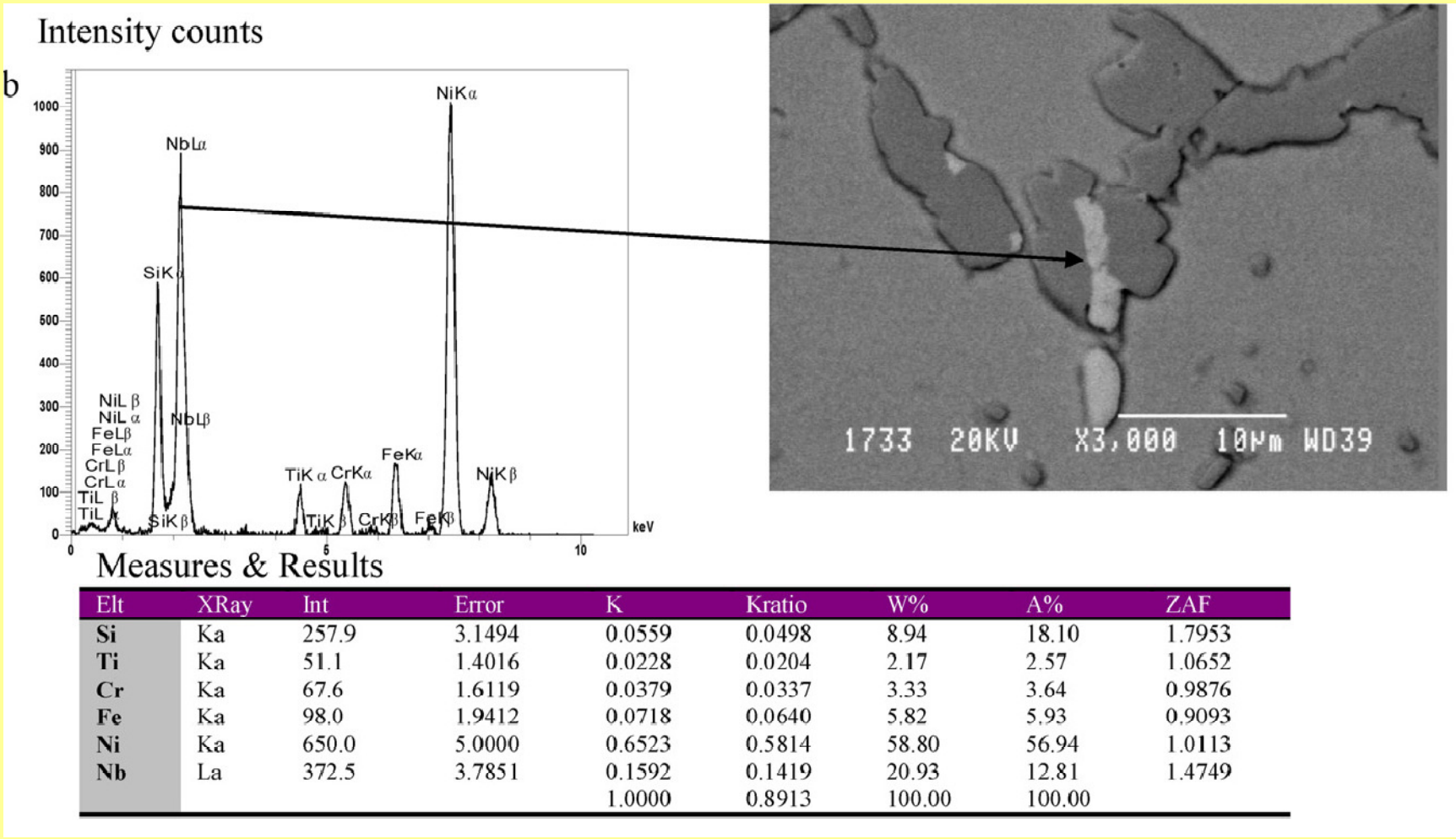
Back scattered image of primary dendritic boundary carbide showing Cr-rich primary carbides at dendritic boundaries in tube 141B. White arrow indicated Nb rich phase.

Measures & Results

Elt	XRay	Int	Error	K	Kratio	W%	A%	ZAF
Cr	Ka	726.7	3.8122	0.9252	0.9212	91.50	92.15	0.9932
Fe	Ka	30.4	0.7802	0.0507	0.0505	5.87	5.51	1.1636
Ni	Ka	10.6	0.4594	0.0241	0.0240	2.63	2.34	1.0965
				1.0000	0.9957	100.00	100.00	

Fig. 4. (a) Back scattered images of primary dendritic boundary carbide showing preferential accumulation of Nb in tube 141B and Cr-rich primary carbides at dendritic boundaries in tube 141B. There is no creep cavitation or voids.

Materials Science and Engineering A 529 (2011) 102– 112

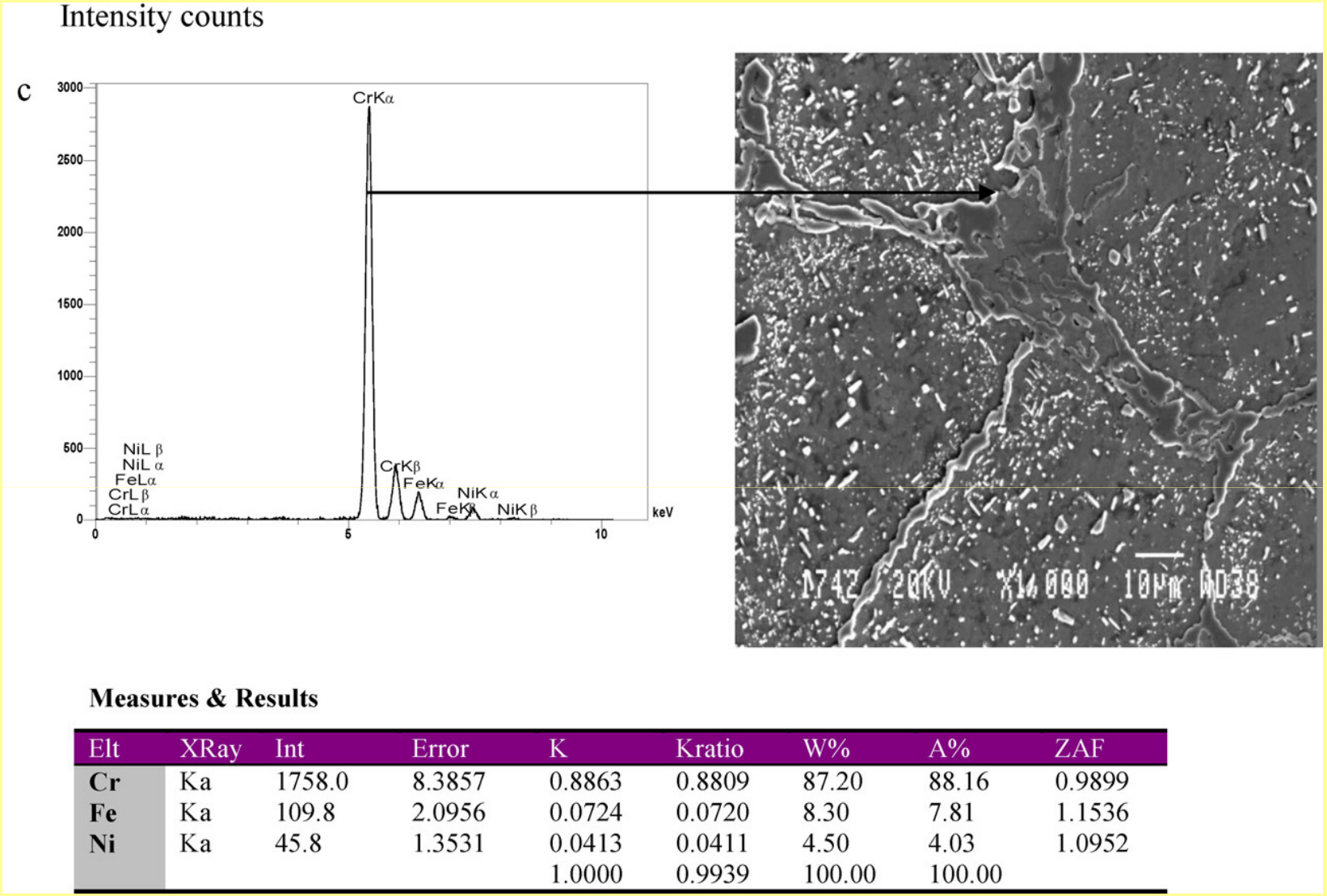


Measures & Results

Elt	XRay	Int	Error	K	Kratio	W%	A%	ZAF
Si	Ka	257.9	3.1494	0.0559	0.0498	8.94	18.10	1.7953
Ti	Ka	51.1	1.4016	0.0228	0.0204	2.17	2.57	1.0652
Cr	Ka	67.6	1.6119	0.0379	0.0337	3.33	3.64	0.9876
Fe	Ka	98.0	1.9412	0.0718	0.0640	5.82	5.93	0.9093
Ni	Ka	650.0	5.0000	0.6523	0.5814	58.80	56.94	1.0113
Nb	La	372.5	3.7851	0.1592	0.1419	20.93	12.81	1.4749
				1.0000	0.8913	100.00	100.00	

Fig.4(b) Back scattered image of primary dendritic boundary carbide showing preferential accumulation of Nb rich phase in tube 141 B.

Materials Science and Engineering A 529 (2011) 102– 112



Measures & Results

Elt	XRay	Int	Error	K	Kratio	W%	A%	ZAF
Cr	Ka	1758.0	8.3857	0.8863	0.8809	87.20	88.16	0.9899
Fe	Ka	109.8	2.0956	0.0724	0.0720	8.30	7.81	1.1536
Ni	Ka	45.8	1.3531	0.0413	0.0411	4.50	4.03	1.0952
				1.0000	0.9939	100.00	100.00	

Fig.4(c) SEM image of primary dendritic boundary carbide showing blocky Cr-rich primary carbides at dendritic boundaries in tube 103B. There is no creep cavitation or voids.

Materials Science and Engineering A 529 (2011) 102– 112

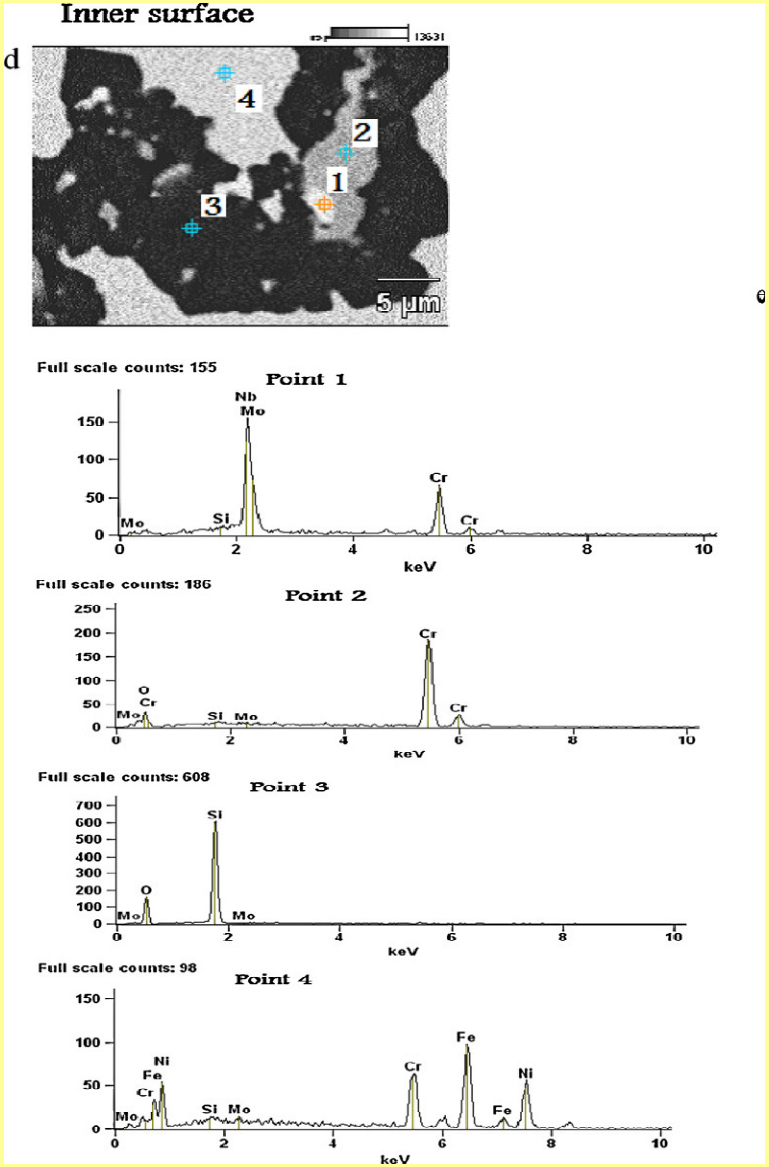


Fig.4(d) EDX analysis of oxide deposit at the inner surface of the service exposed primary reformer tube.

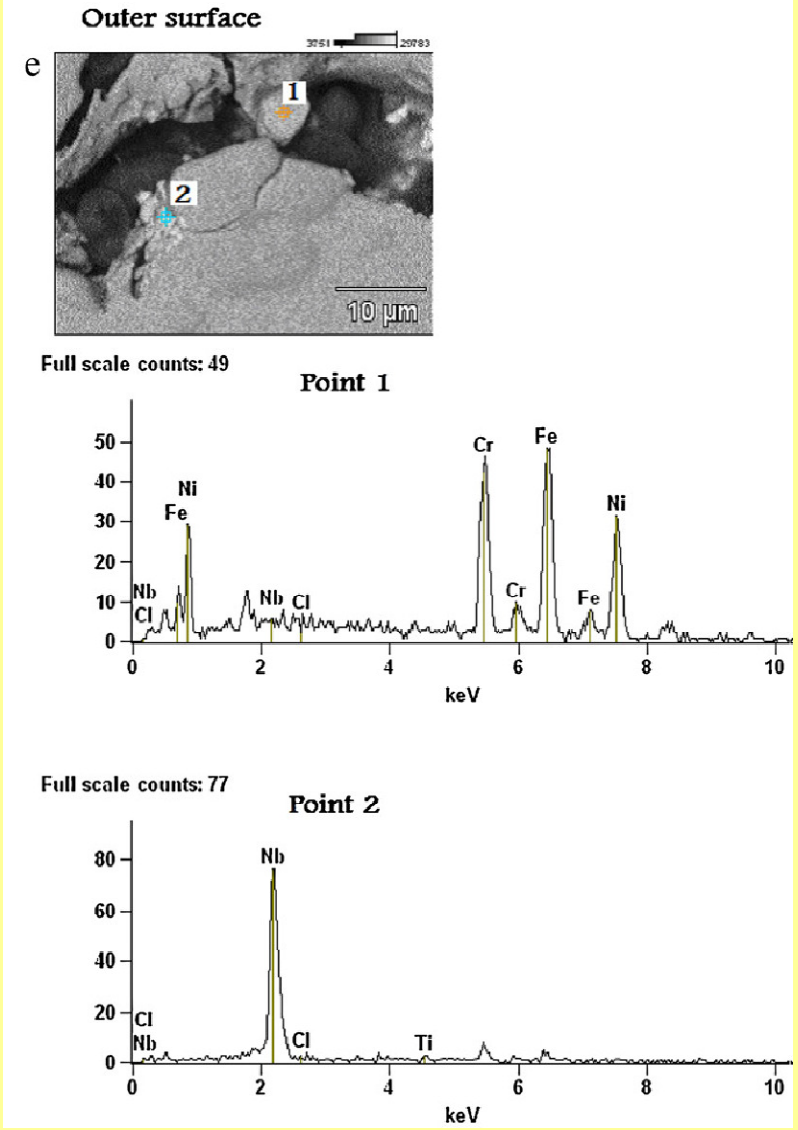


Fig.4 (e) EDX analysis of oxide deposit at outer surface of the service exposed primary reformer tube.

Materials Science and Engineering A 529 (2011) 102– 112

Materials Science and Engineering A 529 (2011) 102– 112

Table 3. Hardness measurements of the service exposed reformer tube

Sl No	Sample Identification	Vickers Hardness Number (VHN)	Vickers Hardness Number from NRIM Data [22] (VHN)
1	Tube no 141 M	214	168-210
2	Tube no 103 M	218	
3	Tube- no 103 B	218	
4	Tube- no 141 B	173	

B- Bottom portion of the tube
M-Middle portion of the tube

Table.4 Tensile test data of service exposed reformer Tube141

Sample Identification	Temp °C	0.2% PS (MPa)	UTS (MPa)	%EL	%RA
Tube no 103 B	900	74	91	18	38
Tube no 103 B	850	92	111	21	40
Tube no 103 B	800	124	141	28	46
Tube no 141 B	900	77	93	19	40
Tube no 141 B	850	95	118	23	40
Tube no 141 B	800	128	145	29	49
Tube no 103 B	25	257	373*	4.6	0.05
Tube no 141 B	25	259	392*	5.0	0.09

***Specimen fractured before reaching UTS**

Materials Science and Engineering A 529 (2011) 102– 112

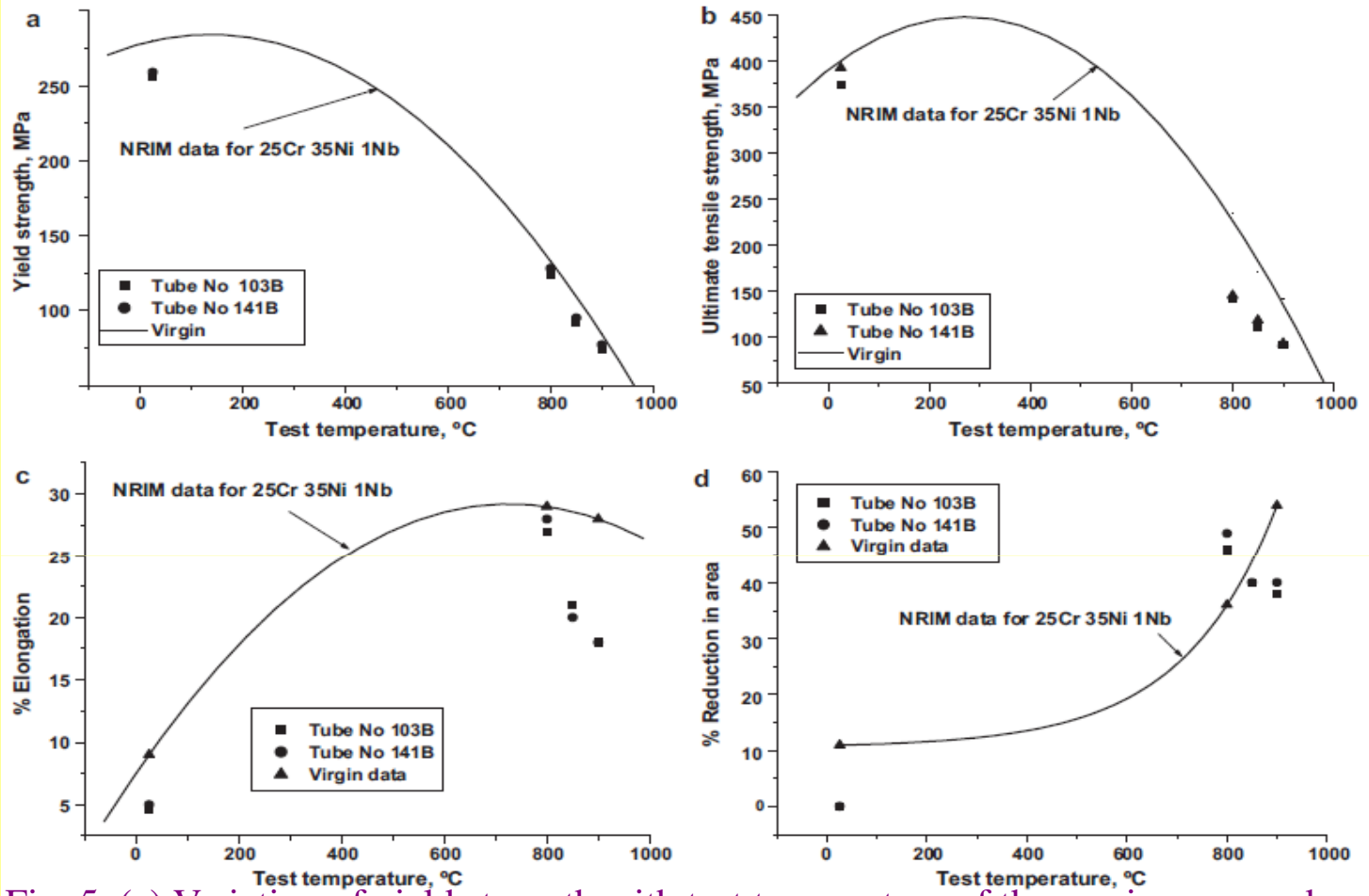


Fig. 5. (a) Variation of yield strength with test temperature of the service exposed reformer tube. (b) Variation of ultimate tensile strength with test temperature of the service exposed reformer tube. (c) Variation % elongation (EL) with test temperature of the service exposed reformer tube. (d) Variation % reduction in area (RA) with test temperature of the service exposed reformer tube.

Materials Science and Engineering A 529 (2011) 102– 112

Table.5 : Results of accelerated creep rupture tests of the service exposed reformer tube

Sample identification	Stress, MPa	Temp, °C	Rupture time, h	% E.L	% R.A
Tube no141-B	63.33	900	11	24	64
Tube no141-M	48	900	1004	9	41
Tube no 141-B	48	900	66	23	70
Tube no 141-B	48	900	754	5	28
Tube no141-M	40	940	497	12	46
Tube no 141-B	40	940	421	9	40
Tube no141-M	32	980	1137	6	24
Tube no 141-B	32	980	1090	5	21
Tube no 103-B	48	900	500	18	32
Tube no103-M	48	900	161	17	66
Tube no103-M	40	940	180	18	67
Tube no 103-B	40	940	356	17	27
Tube no 103-B	32	980	446	10	19
Tube no103-M	32	980	423	19	42

B- Bottom portion of the tube
M-Middle portion of the tube

Materials Science and Engineering A 529 (2011) 102– 112

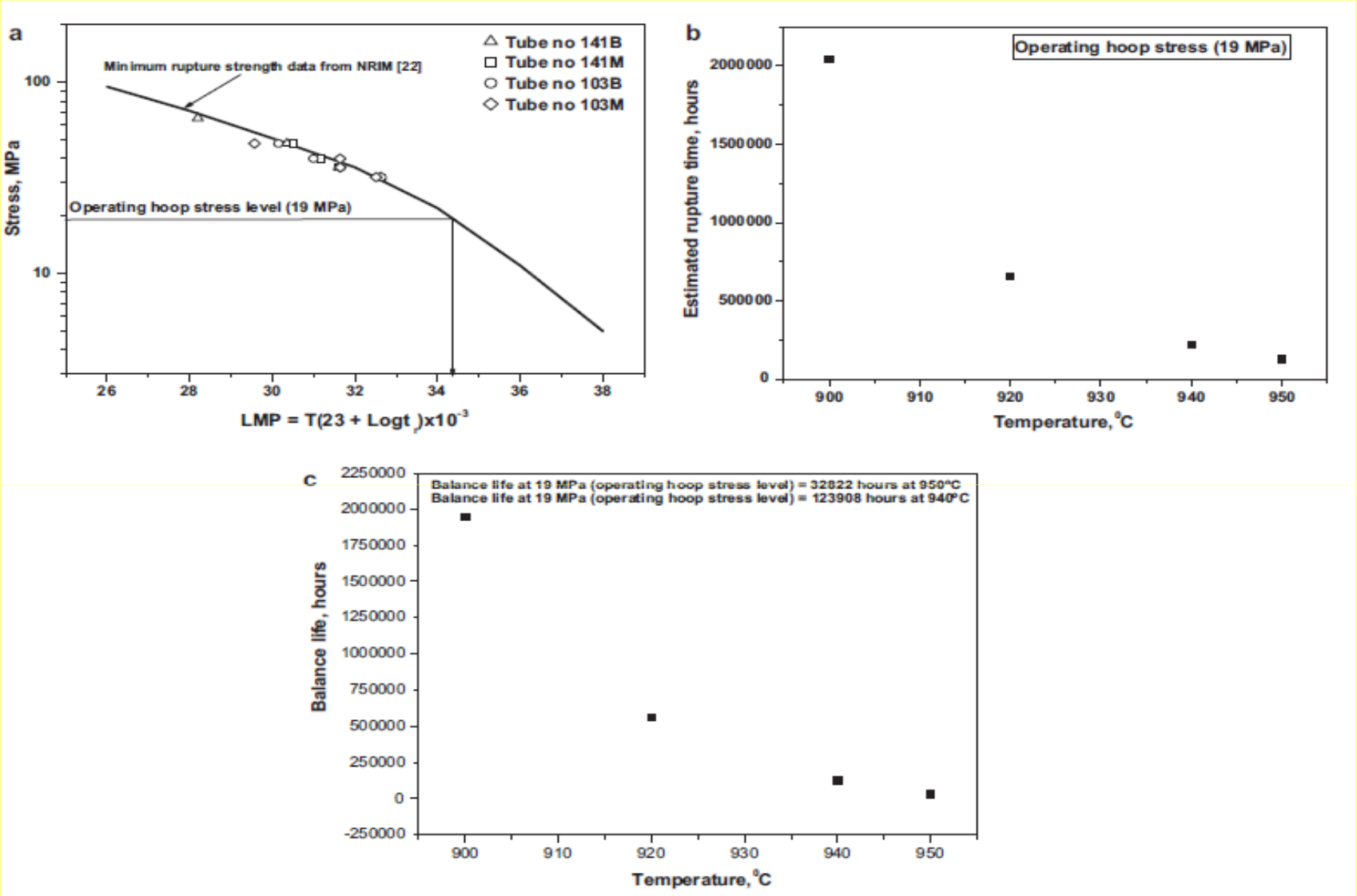


Fig. 6. (a) Stress versus LMP plot of the service exposed 35 Ni–25 Cr–1 Nb–Ti primary reformer tubes in the present investigation. (b) Variation of estimated rupture time with temperature for the service exposed 35 Ni–25 Cr–1 Nb–Ti primary reformer tubes. (c) Variation of balance life with temperature for the service exposed 35 Ni–25 Cr–1Nb–Ti primary reformer tubes.

Materials Science and Engineering A 529 (2011) 102– 112

Summary of results

•Barring development of corrosion cracks and decarburization of the inner and outer walls of the tube, the microstructure of the service-exposed alloy was free from any signs of deterioration. In general, a columnar type of structure was observed having decarburization layers both at internal outer walls or at surfaces. The primary carbide network consisted of chromium-rich $Cr_{23}C_6$ and niobium-rich carbides as intra-dendritic carbides, with some nickel and silicon in it. Presence of significant amount of silicon and nickel at the light grey precipitate confirms that partial conversion of NbC phase to Nb–Ni–Si had occurred. The inter-dendritic crack originated from the inner wall surface. The healthy region of the tube is the mid section of the tube, where Nb rich carbides are seemed to be coagulated and coarsened and are present in the intra dendritic region.

•There was overheating in the bottom region of the tube, as SEM image of the same revealed coarse carbides at dendritic boundaries and disappearance of fine intra dendritic precipitation.

•There was also evidence of corrosion led cracking from outside surface. It is of a highly localised nature as borne out by the fact that the microcracks were absent and no creep cavitation was observed either in isolated or in aligned formthroughout the section of the tubes.

•Oxide deposit analysis of both inner and outer surfaces has revealed that significant increase of Cr, Ni, Si and Nb has occurred at the deposit in the form of oxide.

•SiO_2 deposited in primary grain boundary is possibly rejected from carbide solid solution. At the inner surface deposit of the tube presence of SiO_2 is found to be more than that of the outer surface of the tube.

•The outer surface scale also contained an appreciable amount of chlorine which possibly had come from the internal working fluid i.e. steam.

•EDX analysis has proved that chlorides of alkaline materials are responsible forthe cause of stress corrosion cracking.

•It is therefore, recommended that the internal working fluid should be free from excess chlorine.

•The main damage mechanism for reformer tube is the combination of thermal stresses and internal pressure stresses. This combination of stresses causes creep damage that typically develops at the inner diameter or just below the internal diameter surface. This is the reason as to why more carbide depleted zone is observed at the inner surface than that of the outer surface.

•Analysis of tensile data revealed that there is some deterioration in yield stress (0.2% Proof Stress), ultimate tensile strength of the service exposed primary reformer tubes compared to those of the virgin tube reported in literature which clearly establishes the fact that the material has become softened due to prolonged service exposure and overheating mainly at the bottom portion of the tube. This is also apparent from presence of coarse carbides at dendritic boundaries and disappearance of fine intra dendritic at the bottom portion of the tube. However, the deterioration is within the specified limits.

• There is evidence of 25 ◦C embrittlement of the service exposed tubes which has also been reflected in the 25 ◦C tensile ductility values, observed mainly because of service ageing and overheating.

Reference: Materials Science and Engineering A 529 (2011) 102– 112

Materials Science and Engineering A 529 (2011) 102– 112

•There was no evidence of creep cavitation and voids, therefore only as far as creepstrength and residual life at 950 ◦C/19 MPa is concerned, there is noappreciable degradation due to service exposure and it isjustifiedthat it possible to obtain an additional minimum balance life of 3.7 years for the 11 years service exposed primary reformer tubes. This is valid only if there is no evidence of any localised damage in the form of surface cracks, cavitation or dents and overheating of the tubes resulting in early onset of creep damage.

•Another check for safety of the service exposed tubes, similar to the current work, in terms of residual life is recommended to be carried out after expiry of about 1.5 years of service life from the view of economical and safety reasons. Also during shut down of the plant, NDT (nondestructive) tests viz. Dimensional (thickness and diameter)measurement, hardness measurement and in situ metallographymay be carried out to assess the condition of the materials for their future serviceability.

CASE Study 3

Damage assessment of service exposed reactor and distillation column materials of a petrochemical industry

Nilima Roy, Krishna Guguloth, Ashok Kumar Ray,

Eng. Fail. Anal 28 (2013) 289–301.

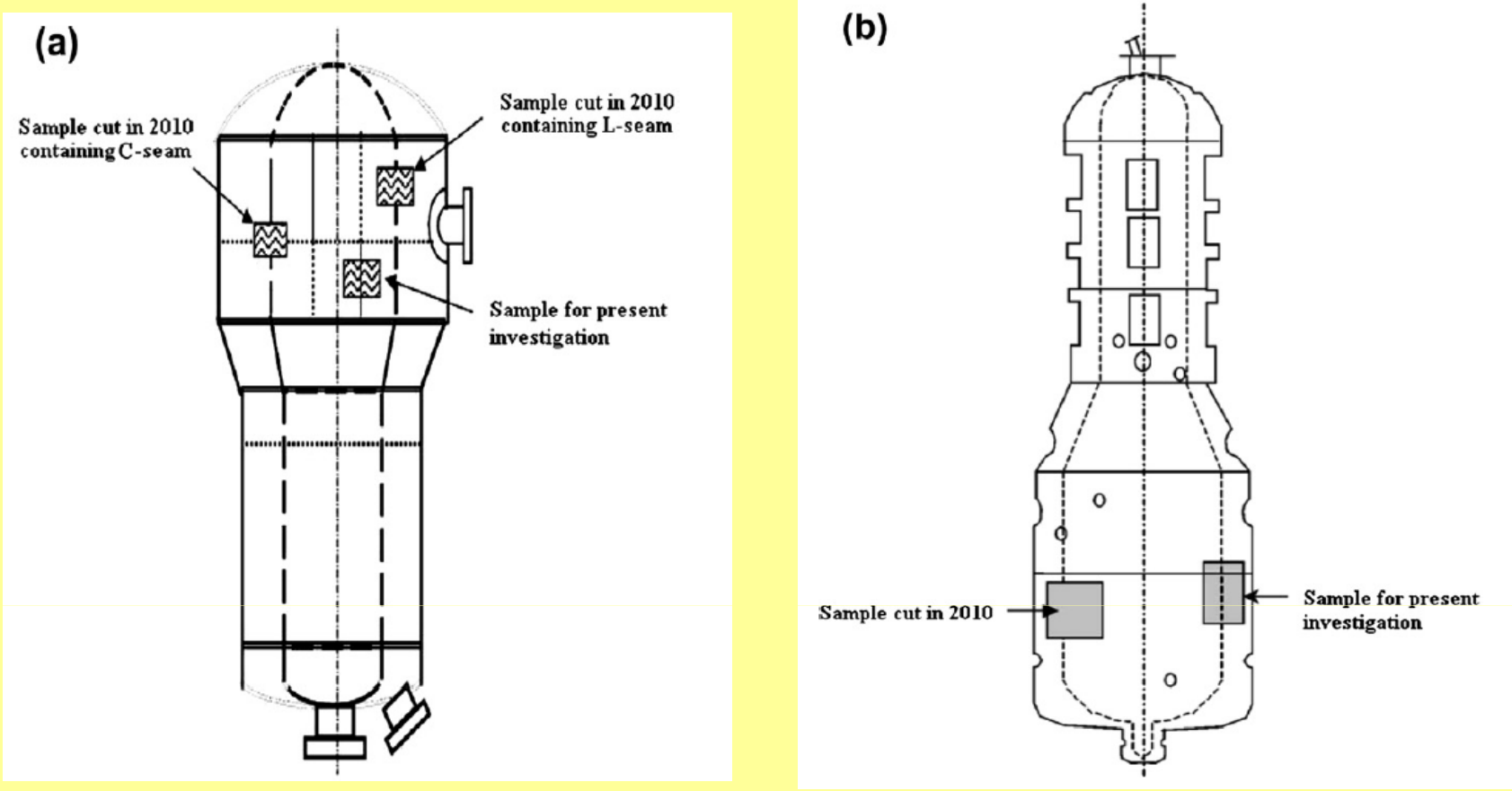
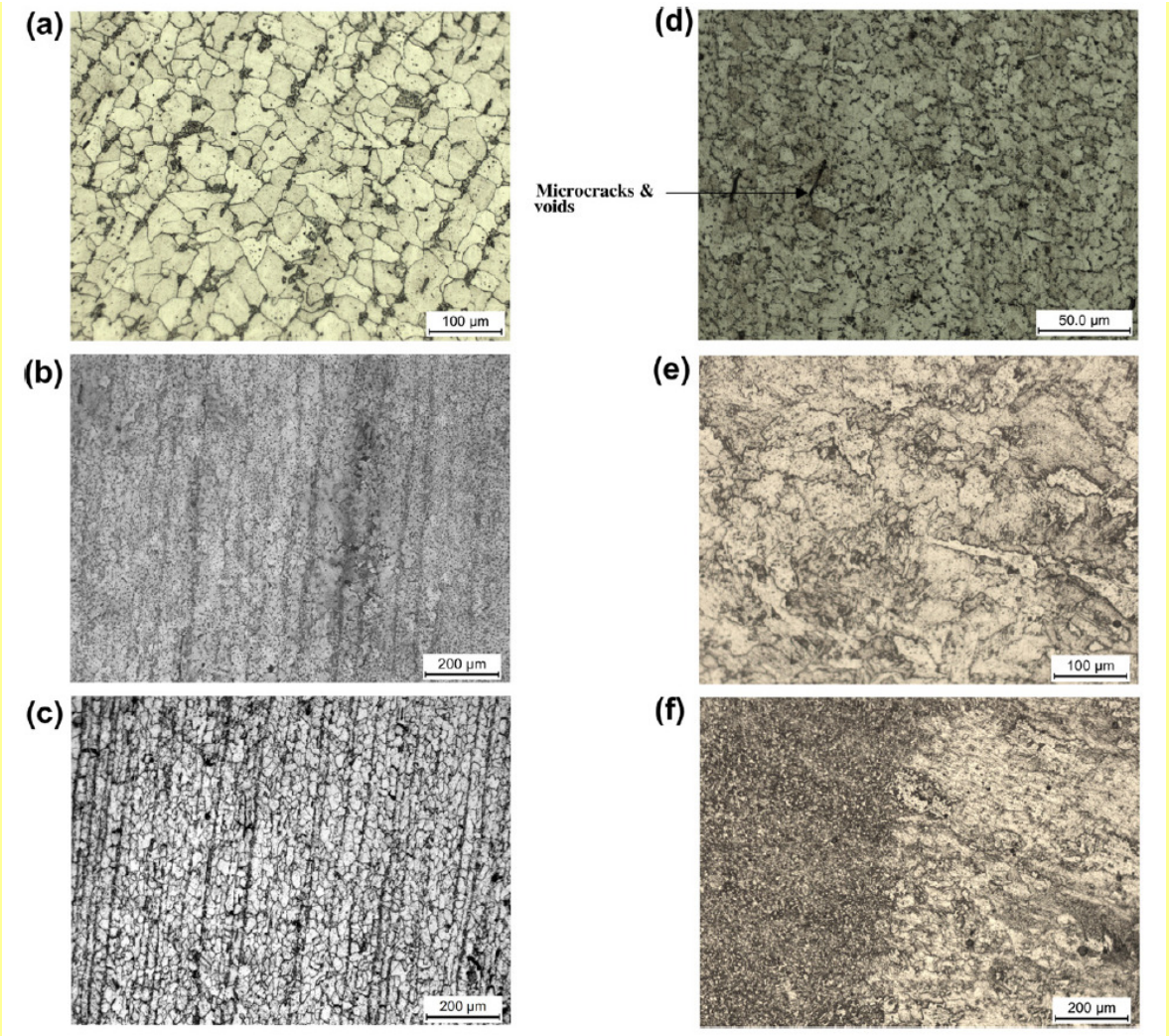
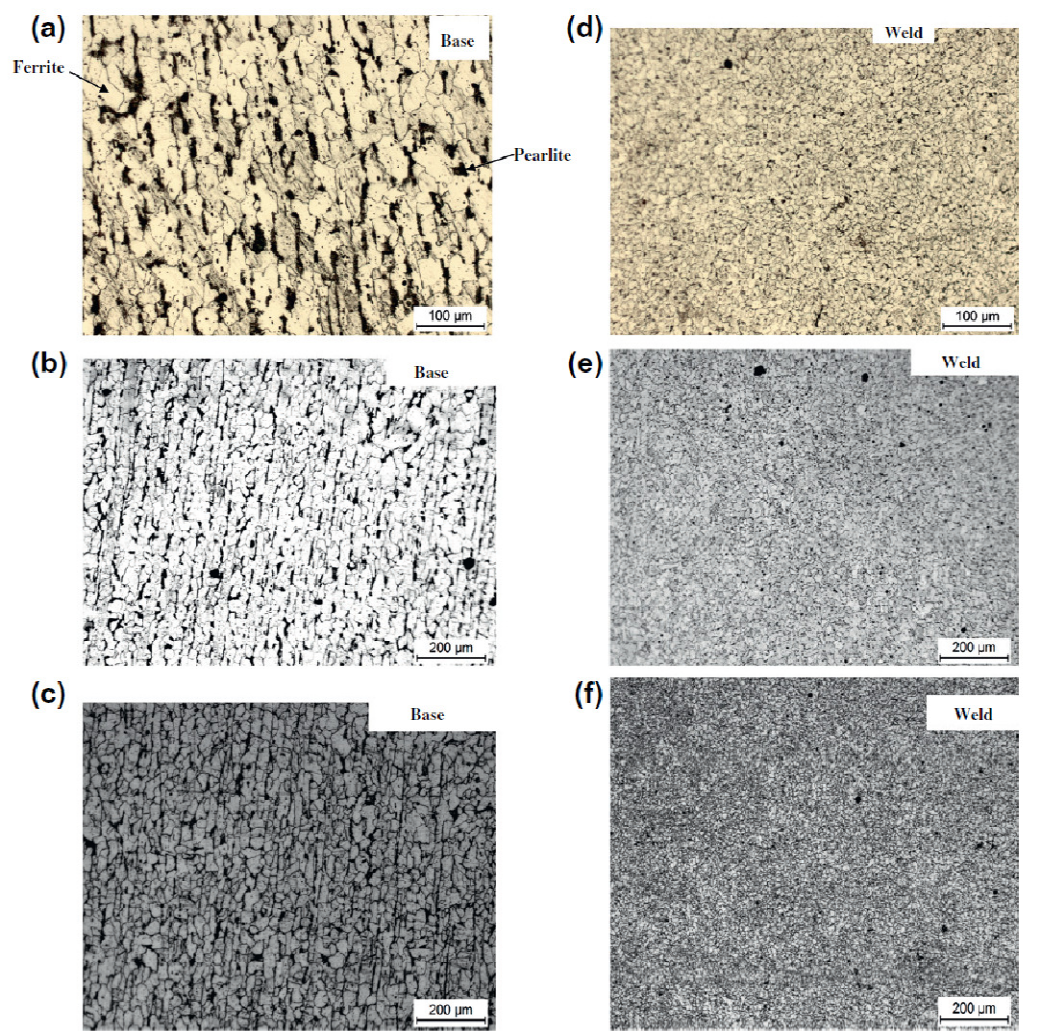


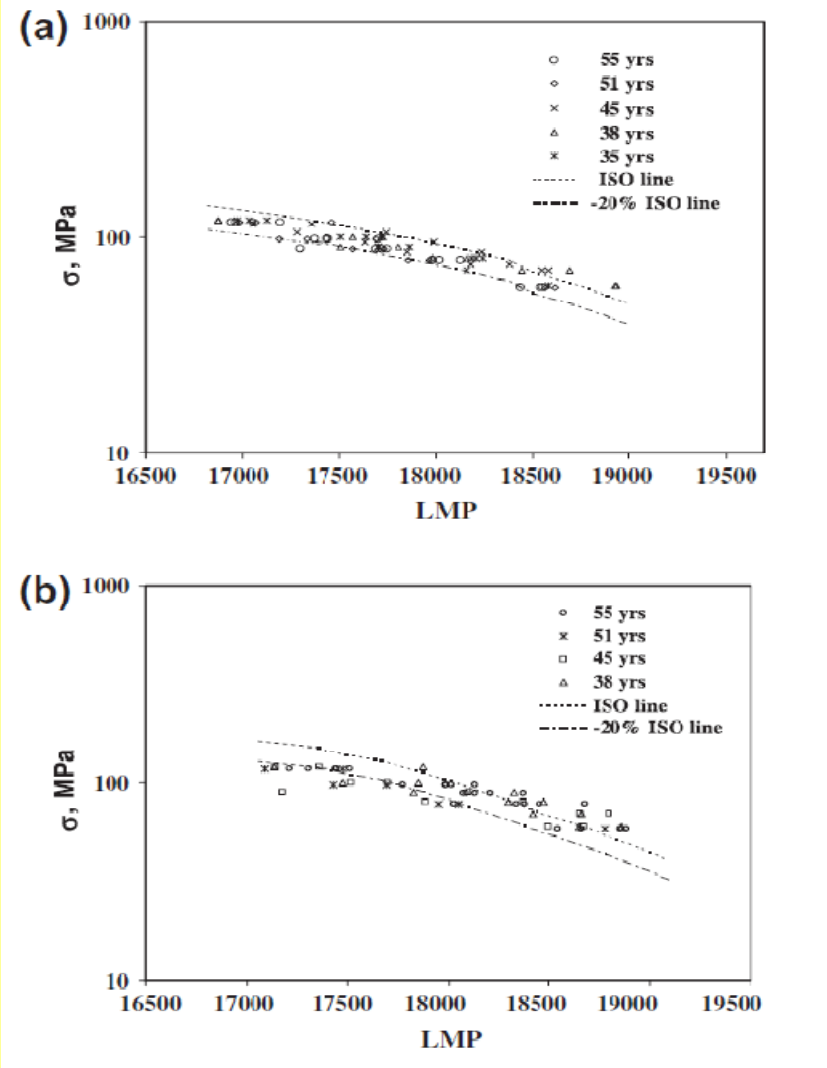
Fig. 1. Schematic of (a) CCU reactor and (b) FPU column material.



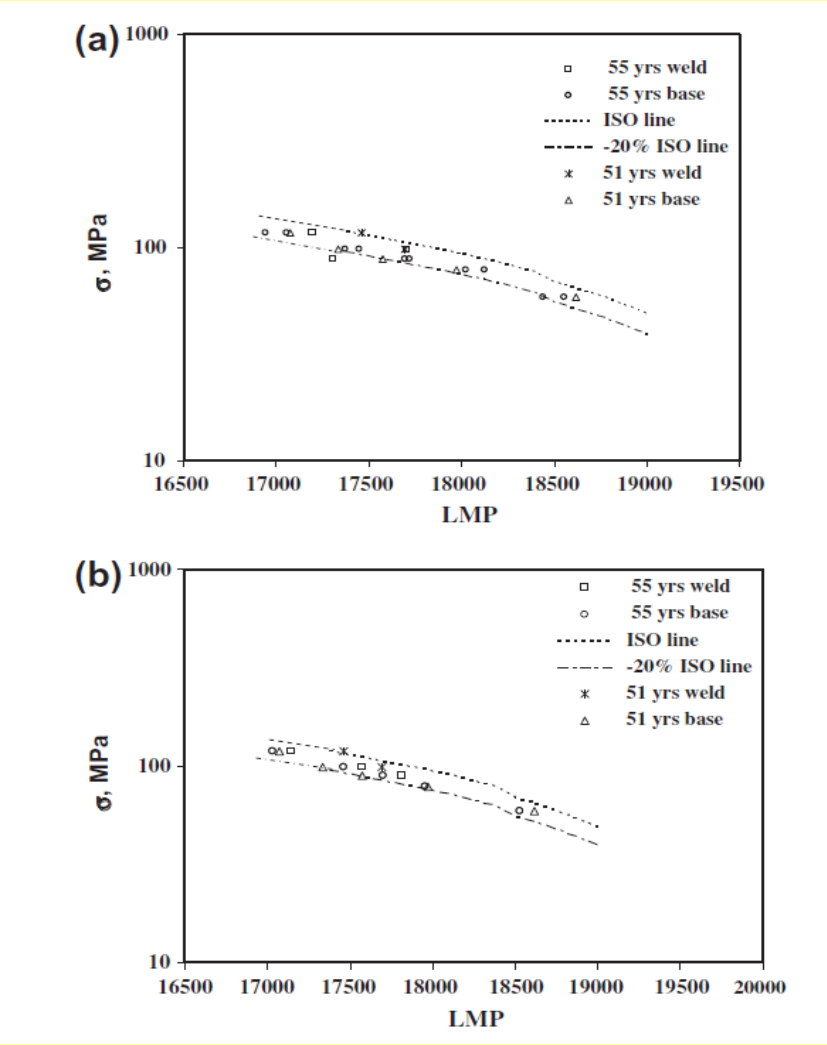
Optical micrograph of service exposed CCU reactor (a) base material in as received condition showing ferritic pearlitic structure. (b) base material in crept condition at 78 MPa/ 515°C showing very fine grain structure. (c) base material crept at 98 MPa/ 515°C showing graphite nodule associated with micro-cracks. (d) weld material in as received condition showing micro-cracks and voids. (e) weld materials crept at 78 MPa/ 515°C showing coarse grains and graphite nodules in the base region and (f) showing transition zone of fine grains in weld region and coarse ferrite (white) grains in base metal regions[



Optical micrograph of service exposed FPU column (a) base material in as received condition showing ferritic pearlitic structure. (b) base material in crept condition at 78 MPa/ 515°C showing elongated grains of coarse ferrite (white) and dispersed pearlite (dark). (c) base material crept at 98 MPa/ 515°C showing ferritic pearlitic structure. (d) weld material in as received condition showing ferritic pearlitic structure. (e) weld material crept at 78 MPa/ 515°C showing fine grains of ferrite(white) and pearlite (dark) and (f) weld material crept at 98 MPa/ 515°C showing showing fine grains of ferrite(white) and pearlite (dark)

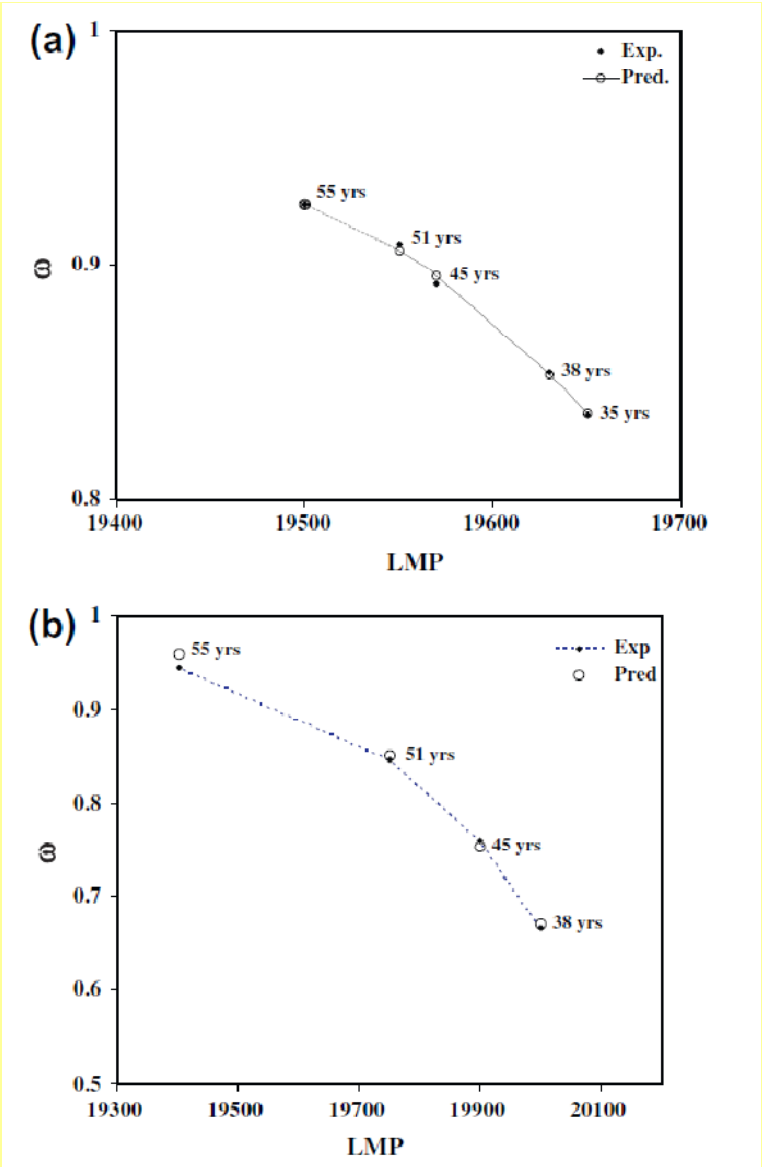


Stress rupture plot for service exposed (a) CCU reactor and (b) FPU column material

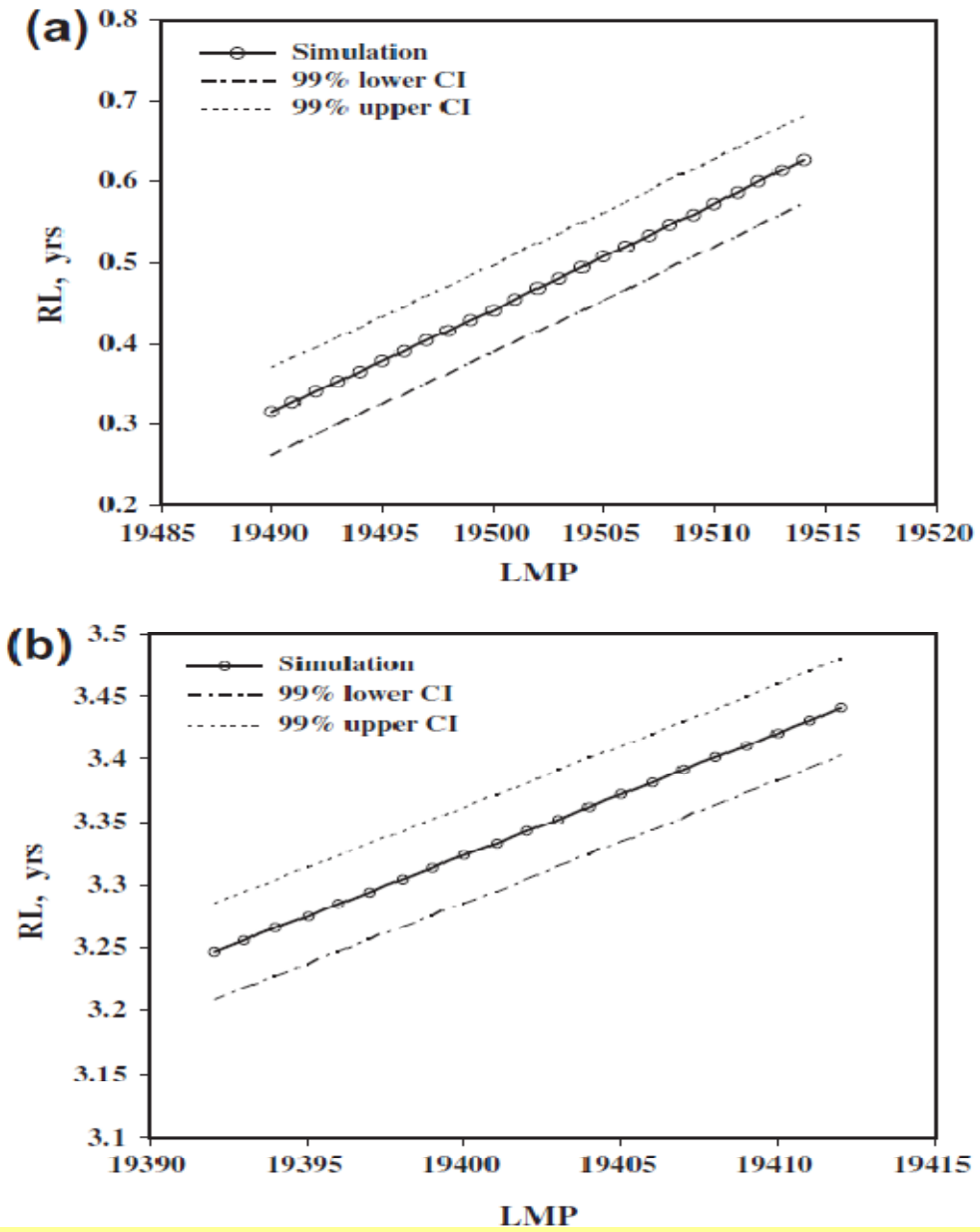


Comparison of rupture data generated in 51 years and 55 years : (a) CCU reactor and (b) FPU column material

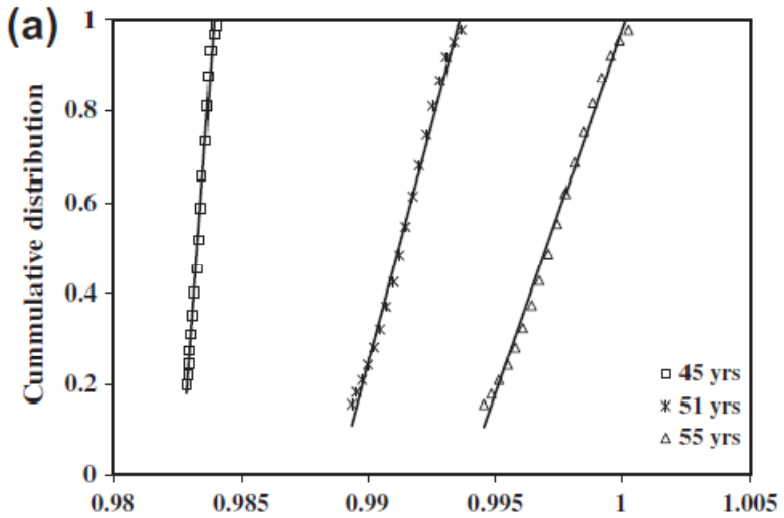
$$\omega = a_0 + a_1 \mathrm{LMP} + a_2 \mathrm{LMP}^2$$

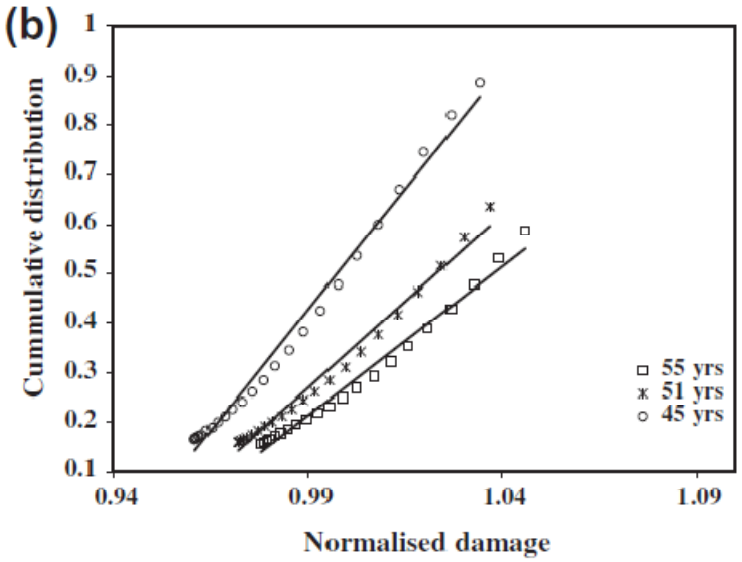


Comparison of experimental and predicted creep damage from of various shut down for (a) CCU reactor and (b) FPU column material

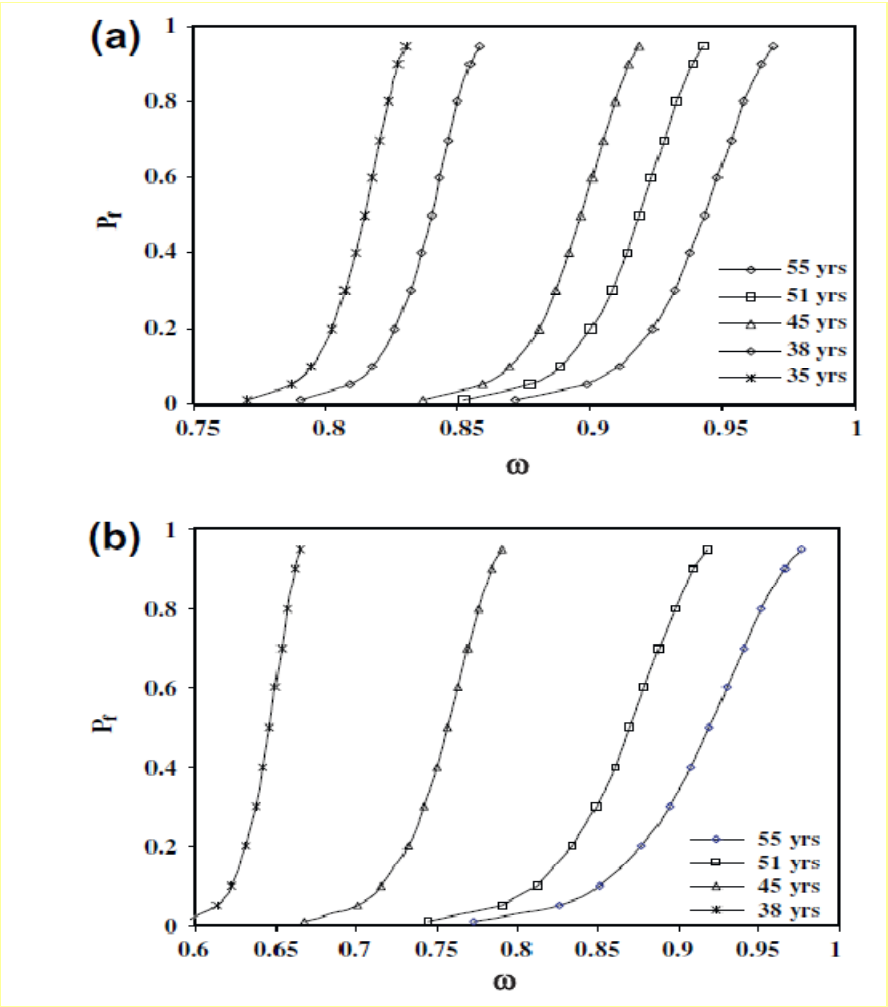


Variation of LMP with remaining life calculation for (a) CCU reactor and (b) FPU column material





Normalized creep damage using Eqn (6) follows Weibull distribution: (a) CCU reactor and (b) FPU column material



Creep damage distribution for various service exposure: (a) CCU reactor and (b) FPU column material .

Nilima Roy, Krishna Guguloth, Ashok Kumar Ray,

Eng. Fail. Anal 28 (2013) 289–301.

Table 2 Remaining life Assessment of 55 years service exposed CCU reactor (ASTM A201 Gr.A) and FPU column (ASTM A285 Gr.C) material with 99 % confidence limit

Component (service exposed)	Temp (^oC)	RL, yrs	Confidence Interval (CI)	Lower CI	Upper CI
CCU reactor	515	2.4	99 %	2.33	2.48
	520	0.47		0.42	0.52
column	515	4.78	99 %	4.73	4.83
	520	3.34		3.3	3.38

Conclusions

Larson-Miller Parameter can also be used to estimate the creep rupture damage for different operating condition, such as operating temperature. Based on accelerated creep rupture tests, service exposed CCU reactor and FPU column materials have balance lives of 2.4 and 4,78 years respectively.

Monte-Carlo simulation has been carried out to predict remaining life for exposed CCU reactor and FPU column materials with 99% confidence level.

Normalized creep damage can be well-approximated with Weibull distribution. It is observed that the distributions shift towards the higher range of damage with increase in service exposure time in case of CCU reactor and FPU column materials.

Thank You



and ε_r , t_r $\dot{\varepsilon}_m$ are rupture stain, time to rupture and minimum creep rate respectively. The product $\dot{\varepsilon}_m t_r \equiv \varepsilon_s$ is the Monkman-Grant constant. λ is a significant parameter in assessing the susceptibility of a material to localized cracking at strain concentrations and is also suggested as a better measure of creep ductility [16-18]. Its value for engineering alloys ranges from 1 to about 20.

$$\omega = 1 - (1 - \frac{t}{t_r})^{\frac{1}{\lambda}} \qquad (4)$$

Eq. (4) defines a generalized creep damage relationship for estimating creep life fraction consumed at any given time. However, this approach does not consider the scatter that is inherent in any creep test. It would be highly beneficial if estimation of remaining life of component could effectively be positioned within the scatter band of creep strain time data.